UNIVERSITY OF OKLAHOMA

GRADUATE COLLEGE

AN EXPERIMENTAL INVESTIGATION INTO USING ELECTRO-CHEMICAL PROPERTIES TO MEASURE PERMEABILITY IN LOW PERMEABILITY FORMATIONS

A THESIS

SUBMITTED TO THE GRADUATE FACULTY

in partial fulfillment of the requirements for the

Degree of

MASTER OF SCIENCE IN NATURAL GAS ENGINEERING AND MANAGEMENT

By

TABISH ABDUL KADAR KAZI
Norman, Oklahoma
2016

AN EXPERIMENTAL INVESTIGATION INTO USING ELECTRO-CHEMICAL PROPERTIES TO MEASURE PERMEABILITY IN LOW PERMEABILITY FORMATIONS

A THESIS APPROVED FOR THE
MEWBOURNE SCHOOL OF PETROLEUM AND GEOLOGICAL ENGINEERING

BY

_____
Dr. Mashhad Fahes, Chair

_____
Dr. Suresh Sharma

_____
Dr. Maysam Pournik

To my family and friends

Acknowledgements

I am immensely grateful to my family for their unwavering support and encouragement; they have not only provided me with invaluable resources but have also constantly inspired me to strive for excellence. For this, I am deeply indebted to them.

I express my deepest appreciation and gratitude toward Dr. Mashhad Fahes for her guidance, support, and invaluable knowledge. Her mentorship throughout my Master's program has been crucial to my development as a researcher. I am also grateful to Dr. Suresh Sharma and Dr. Maysam Pournik for investing their time in my work by serving as a committee member, despite their busy schedule. I would like to extend a special thanks to Gary stowe for his technical support with lab equipment. I would like to thank my fellow lab mates Mohamed Mehana, Mohammed al Salman, and Shashwat Agarwal, who graciously contributed time by lending insight, and engaging in technical discussion. I would also like to acknowledge all my friends including Dannelle, Soham, Abhijeet, Sumeer, Fatema, Nidhi, Nauman, Anvit, Diken, Maulin, Richa and Adrienne for making this place a home away from home with their love and emotional support. Thank you, guys, for always being there during my highs and lows.

Table of Contents

List of Tables

List of Figures

Abstract

Permeability is one of the most important property in the study of rock formations. Different permeability measurement techniques have been used in the industry, some of which are based on modelling while others on experiments. The most widely used techniques are mercury intrusion porosimetry, GRI (gas research institute) technique and pressure pulse decay. These techniques have achieved varying amounts of success depending on the kind of formation. The main factor which binds these techniques is the parameter of pressure without which permeability measurements cannot be done. All these methods require pressure dependent equipment, pressurized cylinders, and special core holders etc. which are highly expensive.

In this study, we seek answers to the possibility of substituting the pressure parameter with an electro-chemical parameter like conductivity using a simple, cost effective setup. The study is based on the principle of osmosis and diffusion and is carried out on Indiana limestone, Sister Berea sandstone, Grey Berea sandstone and shale with sample lengths in the range of 0.07-0.1 inches. The tests were conducted in 250 ml beakers and temperature compensated conductivity meters were used for conductivity measurement. Fluids incorporated in this study were, 10%wt. /wt. KCl solution and deionized water. Wax was used as a sealant to prevent flow of fluids around the circumference of the rock samples.

The plots of conductivity readings were generated and analyzed with respect to time. It was observed that for indiana limestone with permeability in the range of 2-5 mD, the chemical equilibrium between different salinity fluids was absent. In case of sister berea with the permeability of 70 mD and grey Berea with the permeability of 130 md, the

smooth path towards chemical equilibrium was observed. In case of shale with permeability of 150 mD, the initial convergence due to diffusion and osmosis was quick which in the later stages of the experiment slowed down. It was also observed that the length of the rock samples has a huge effect on the time taken to reach chemical equilibrium.

1. INTRODUCTION

1.1 Overview

Technological advancements have become a necessity in order to meet the global oil and gas demands, especially with the conventional reservoirs reaching their peak production limit and the need of the time is to exploit the hard to produce unconventional reservoirs. Hydraulic fracturing technology is one such advancement that was initially started as a mere experiment in 1947 and has been developed periodically thereafter, especially successful results in low permeability unconventional formations like shale and limestone. As a result of this, immense research has been conducted to study the properties of these rocks. Permeability of these formations became one of the most important and widely studied property.

1.2 Problem description

In case of low permeability formations, the most widely used methods to estimate the permeability are GRI technique, mercury intrusion porosimetry and pressure pulse decay method. Out of these, GRI technique is carried out on crushed samples in the laboratories (Profice et al., 2011). Mercury intrusion porosimetry (Kamath, 1992) uses mercury injection curves and relates it to permeability. Brace et al., introduced the concept of pulse decay by using it on granites in 1968. In this method, rate of change of pressure pulse is recorded and used to estimate the permeability. These methods are discussed further in chapter 2. One common factor, which binds these methods together, is the use of pressure, which acts as a catalyst and is very important factor in determining rock permeability. The objective of this study is to investigate the possibility of replacing the pressure term

with an electrochemical property such as conductivity and to study the effect of variable flow behavior through the low permeability formations on the electro-chemical properties of the fluid they are in contact with.

The three methods listed above, in general, require specialized core holders, pressurized cylinders and other costly equipment in order to conduct experiments and obtain data. However, to make the research more cost effective, it is desired to eliminate the use of such costly equipment and instead use a simple setup to investigate the possibility of estimating permeability.

2. LITERATURE REVIEW

2.1 Rock Mineralogy

Core samples from formations such as Indiana Limestone, Sister Berea, Grey Berea and Shale are considered within the scope of this study. Indiana limestone is a calcite formation bound together with the grain stone made up of fossil fragments and oolites. This formation has a low permeability (4-57 mD) and high porosity (12-21 %). These rocks primarily contain calcite with a small concentration of quartz. Table 1 shows the mineralogy of Indiana limestone:

Table 1. Mineralogy of Indiana Limestone

Composition	% concentration/mass/volume
$CaCo_3$	97.3
$MgCo_3$	0.4
Al_2O_3	0.5
SiO_2	1.7

Berea Sandstone has a very different pore structure compared to Indiana Limestone. The Upper Berea sandstone unit is widely studied in the core flooding experiments. The grains are finer and well sorted as compared to Indiana limestone. As a result, Berea Sandstone has a higher porosity. Table 2 shows the mineralogy of Berea Sandstone:

Table 2. Mineralogy of Berea Sandstone

Composition	% conc./mass/vol
Quartz	88.9
Clay	3.9
Fieldspar	3.4
Carbonate	2.2
Evaporite	0.5
Others	1.1

Samples from Sister Berea utilized in this study have permeability in the range of 70-90 mD and porosity of approximately 21%. Gray Berea has permeability of approximately 100-130 mD and porosity of 18%.

Table 3. Mineralogy of an Average Shale

Composition	% conc./mass/vol
Quartz	20
Feldspar	8
Carbonate	7
Fe-oxides	3
Clay minerals	59
Other minerals	3

Shale formations are one of the most abundantly found sedimentary rocks in earth's crust. In petroleum geology, organic shale formations are source rocks as well as seal rocks that trap oil and gas (Speight, 2014). The source of sediment for shale formation is the mud deposited on the seabed. Initially, these muds are highly permeable. With time, they subside over and compact into shale formations. Shale is known for its clay content (50-60%) and its low permeability. Shale usually contains clay minerals such as illite, kaolinite, and smectite. In addition to these minerals, they may also contain quartz, chert and feldspar in small concentrations. Other constituents can include organic particles, carbonate minerals, iron oxide minerals and sulphide minerals depending on the environment responsible for shale formation. Different authors have calculated the

average mineralogical composition of shale. Table 3 lists estimates of average mineralogical composition of shale calculated by D.H. Yalon (1961).

2.2 Permeability and its Significance

Shale gas formations are unconventional reservoirs i.e. they are reservoirs having very low permeability. In case of conventional reservoirs, the gas in the interconnected pore spaces is free to move to the well bore. However, in case of shale formations, due to its low permeability, the gas is unable to move freely. Hence, the reservoir has to be mechanically stimulated to increase the permeability and to allow the gas to transport freely into the well bore for production. Beside shale formations, other examples of unconventional reservoirs can be tight gas reservoirs and coal bed methane reservoirs. For shale formations, hydraulic fracturing is the preferred stimulation method. During hydraulic fracturing, large volume of pressurized fluid is injected into the formation to stimulate or fracture the formation within the zone of interest and subsequently, allow the gas from the formation into the wellbore via the fractures. Sand is commonly used as a proppant and is pumped along with the fluid to keep the fracture open. The type of fluid used and its composition depends on the geology of the formation to be fractured. When water is used as a pressurized fluid, a good fraction of it is recollected at the surface (called flow back) and is reused for subsequent fracturing after adequate water treatment.

During the last few decades, another major technology that has been widely used for production of natural gas is called ‘horizontal drilling’. The initial segment of the well is drilled vertically similar to a conventional gas well. The drilling trajectory deviates from the vertical path and to a horizontal trajectory as the drilling continues within the shale formation. This helps in maximizing the number of natural fractures in the shale that are

intersected by the well and these additional fractures allow the gas which was trapped to flow freely once hydraulic fracturing is carried out.

Rock permeability is controlling factor in fluid migration, entrapment and over-burden pressure development. It is one of the most critical parameters for reservoir characterization and the well performance evaluation in tight gas reservoirs (Cheng Cao, 2016). The accurate measurement of permeability in these formations is very important. Rock properties at laboratory and field scale are critical for evaluating the production potential of these reservoirs. Most of the gas is stored in formation matrix, which has very low permeability and may consequently limit the production rate. The importance of permeability in hydrocarbon accumulation has led engineers to investigate the controlling factors.

2.3 Permeability Measurement Techniques

The traditional methods which are used for estimating the permeability of tight gas sands have been described below. Under steady state flow conditions, it is assumed that the pressure gradient is constant and directly proportional to the fluid velocity. This constant as defined by Darcy's law, is the absolute core permeability that is given by,

$$\frac{dp}{dx} = -\frac{\mu}{k} V_x$$

Where,

μ = Viscosity of the fluid (typically in units of centipoise)

k = Permeability of the formation (typically in units of millidarcy)

V_x = Interstitial gas velocity along core length, cm/sec

However, cores with permeability less than 0.1 mD are unlikely to achieve steady state flow in less duration; especially when liquid is the mobile phase. Gas is quite often used in low permeability cores. However, gas flow in tight formations is also affected by non-Darcy effects like gas slippage and inertial flow, which can cause measurement errors. Klinkenberg (1941) studied the gas slippage effects on porous media. It was observed that the permeability to gas is a function of mean core pressure. The Klinkenberg corrected permeability is derived from a straight-line intercept on a plot of measured permeability against reciprocal mean pressure. It is given by,

$$\mathbf{k = k_{\infty}(1 + b\sqrt{\overline{p}})}$$

where,

k_{∞} = Klinkenberg corrected permeability(units)

b = gas slippage factor (units).

Figure 1 is a cartesian plot of inverse mean pressure against the apparent gas permeability.

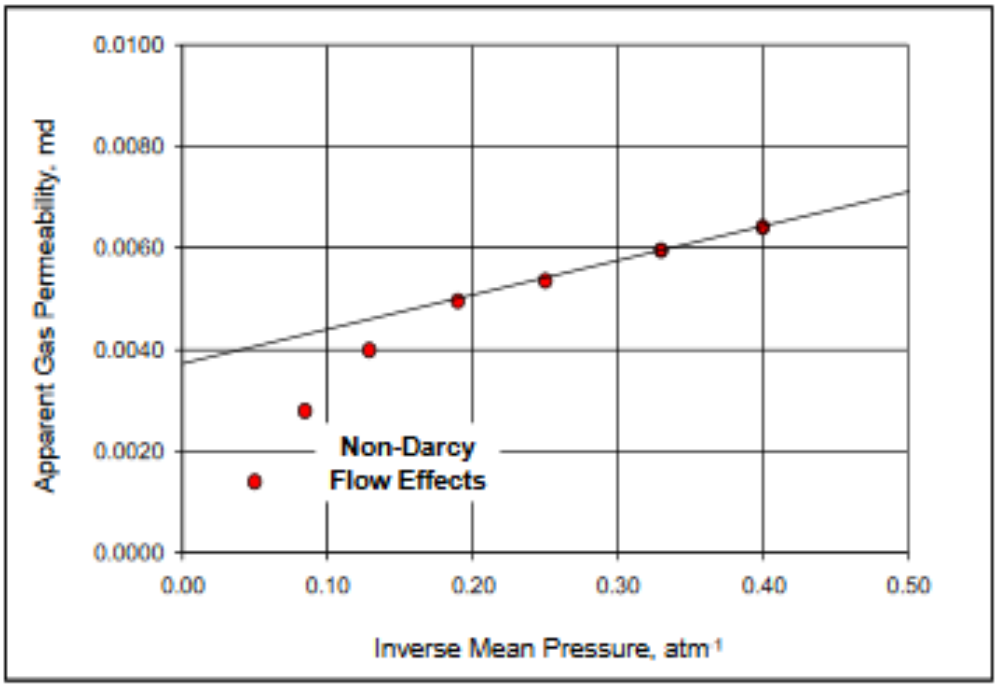

Fig 1. Hypothetical Klinkenberg plot (Rushing 2004)

The plot depicts the non-Darcy flow behavior identified as deviations from the straight line at higher mean pressures. The Klinkenberg permeability is obtained from y-intercept and gas slippage factor is obtained from the slope of the line. Additionally, the plot also identifies the non-Darcy effects at high mean pressures. Rushing (2004) used backpressure to minimize the non-darcy effects. Klinkenberg corrected permeability was measured with backpressure of 0, 46.5 and 146.4 psig. The effects of backpressure were observed in a cartesian plot of slippage-corrected Darcy pressure drop against mass flow rate. Rushing (2004) observed that steady state measurement is more accurate with the

use of finite backpressure (Fig. 2 to 4), as it causes reduction in both gas slippage and inertial effects

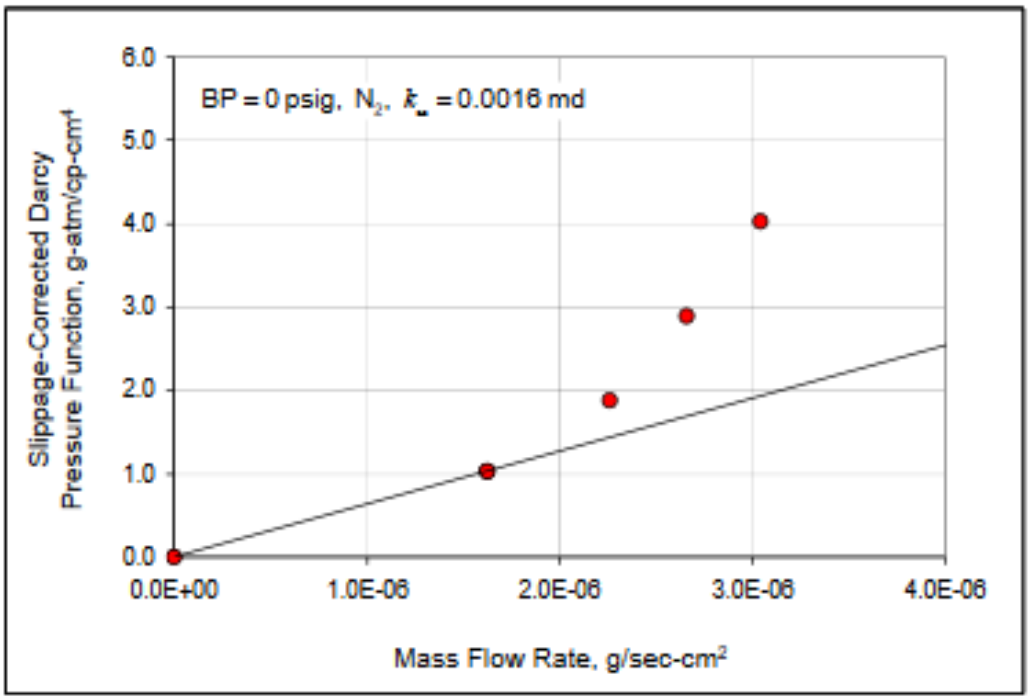

Fig. 2. Plot of slippage-corrected Darcy functions showing effects of backpressure, backpressure=0 psig (Rushing 2004)

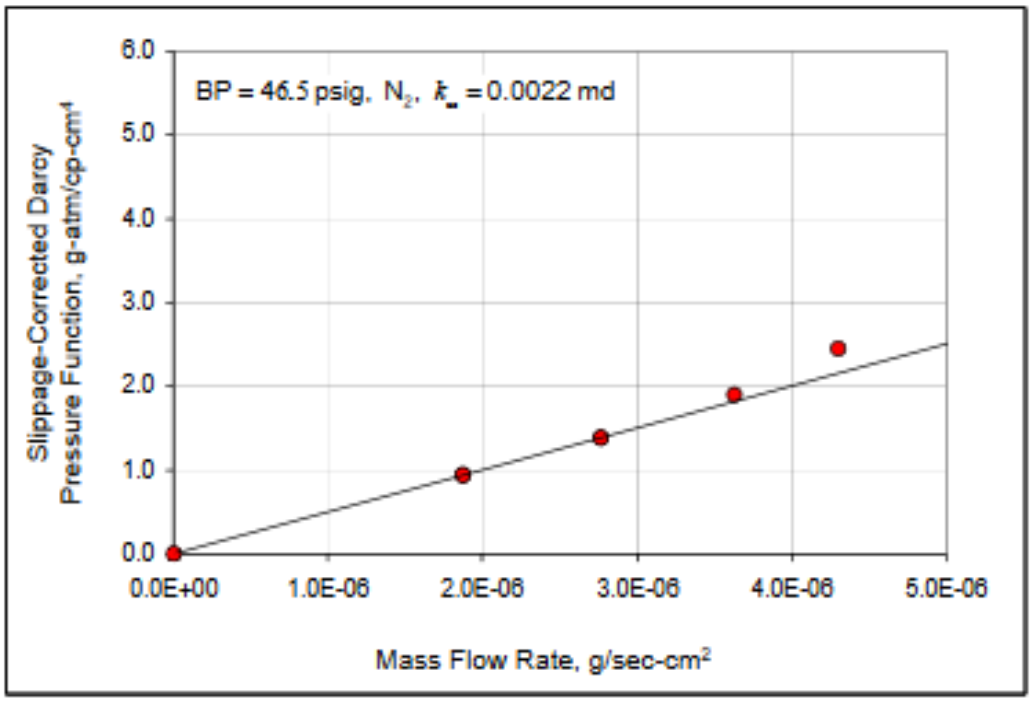

Fig. 3. Plot of slippage-corrected Darcy functions showing effects of backpressure, backpressure=46.5 psig. (Rushing 2004)

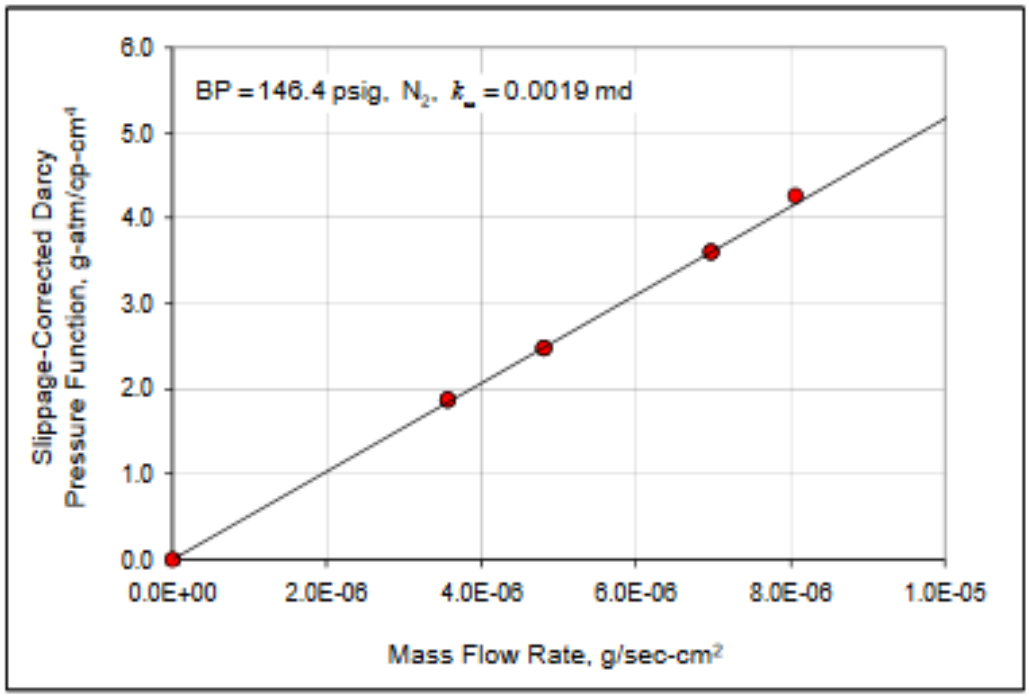

Fig. 4. Plot of slippage-corrected Darcy functions showing effects of backpressure, backpressure=146.4 psig. (Rushing 2004)

This reduction in non-Darcy behavior is due to increase in the overall mean core pressure, which causes the gas to behave more like a liquid phase. The measurement error obtained using this methodology is considerably low. However, due to low permeability of shale, the duration to obtain results using steady state method is considerably high. This, subsequently, reduces the integral efficiency of the steady state system. Hence, it is often required to implement the unsteady state methods of permeability measurements. The three most widely used such techniques for permeability measurement are GRI (Gas Research Institute) technique, mercury injection and pulse decay.

2.3.1 GRI Technique

The commonly used unsteady state method of measuring permeability is the GRI technique. This technique involves using helium as an inert gas that is expanded from the reference cell into sample cell. The gas fills up the pore spaces within the crushed rock placed in sample cell from all directions with cross bedding transfer. This technique, developed by GRI, can be implemented on as-received pore liquids yielding the effective permeability or on dry particles to obtain absolute permeability.

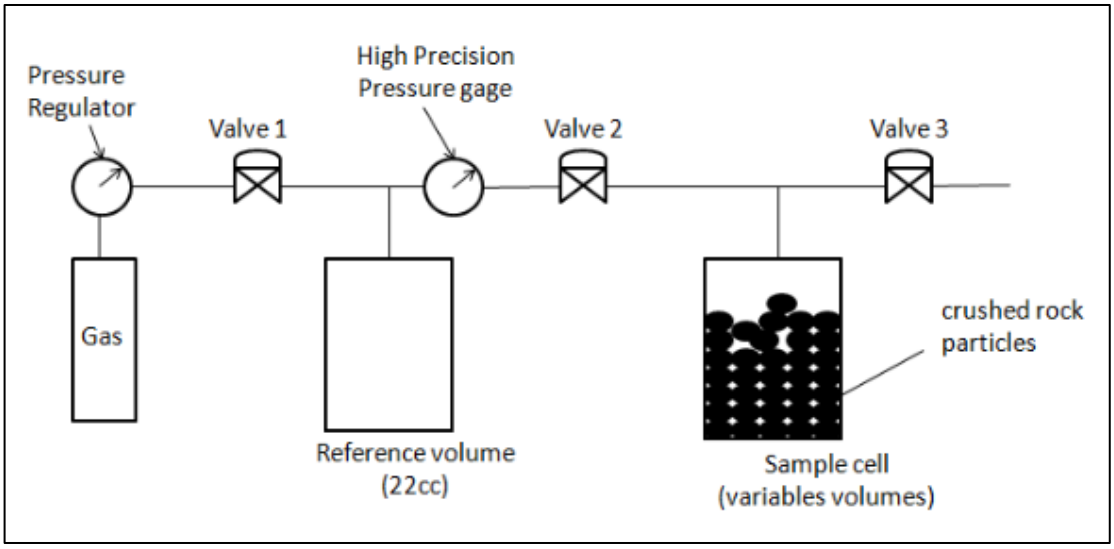

Fig. 5. Schematic of the GRI permeability measurement apparatus (Ali Tinni 2012)

Figure 5 is a schematic of the setup used for permeability measurement using GRI technique.

In this method, a pressure pulse is applied on the unconfined crushed rock particles. Pressure decay cure is obtained as an output which is further analyzed to obtain permeability. Figures 6 & 7 show the recorded pressure data vs time before the valve 2 is opened and the pressure decay plot obtained as an output, respectively.

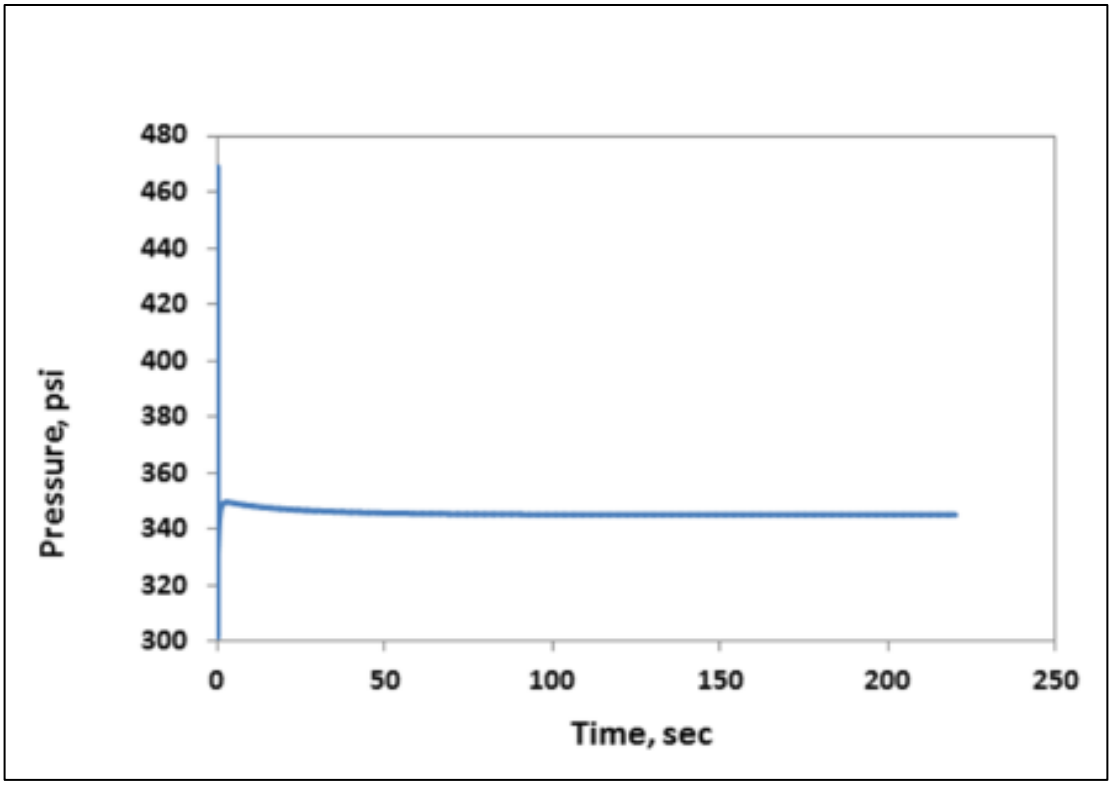

Fig. 6. Pressure data recorded vs time (Ali Tinni 2012)

The GRI method is fast and effective but has of its own drawbacks and limitations. As discussed later, the shale permeability is highly sensitive to net stress. Sondergeld (2010) concluded that the results obtained by GRI technique are inconsistent and are dependent on many variable laboratory factors. Since GRI technique uses crushed samples, it is assumed that crushing the sample removes the micro fractures in the shale, which can be open under test condition but will most likely be closed under reservoir stress condition. Ali Tinni (2012) showed that the micro fractures exist even in finely crushed samples.

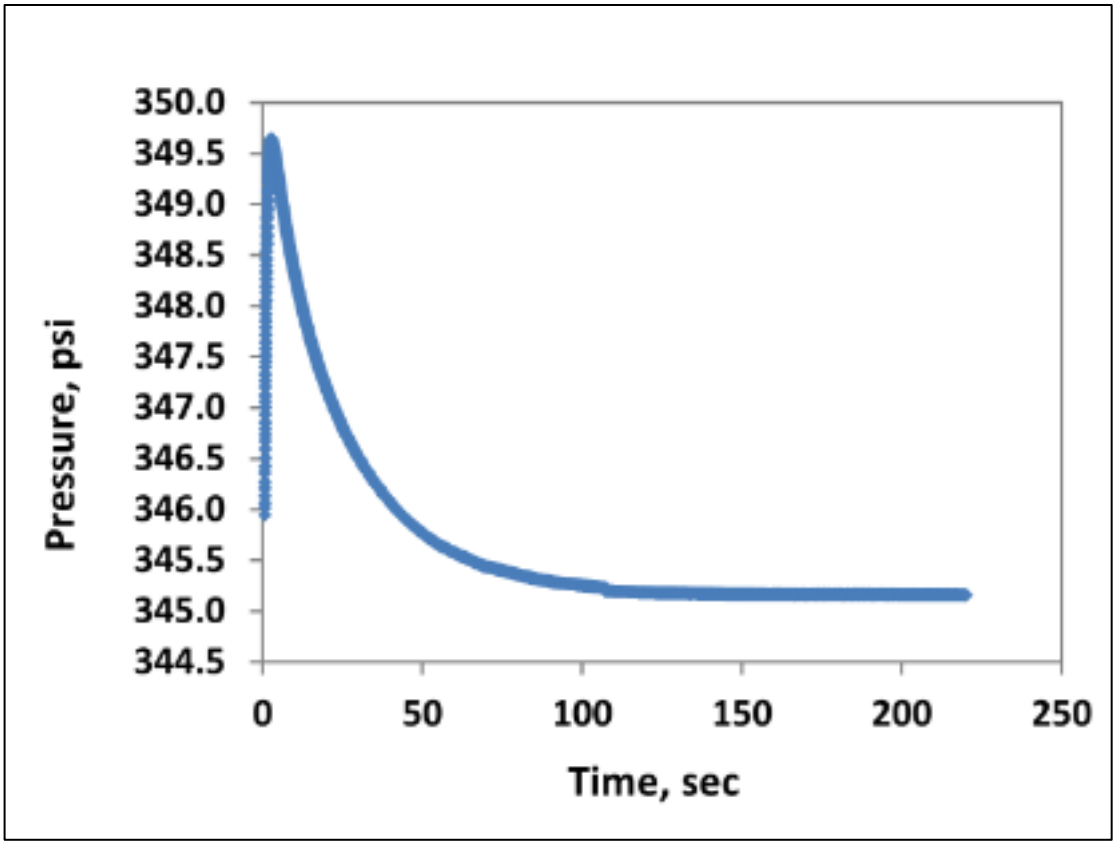

Fig. 7. Pressure decay inside the Shale sample (Ali Tinni 2012)

2.3.2 Mercury Injection

Mercury intrusion is widely used for the determination of total pore volumes and pore size distributions for porous material. Purcell et. al. introduced this technique in 1949.

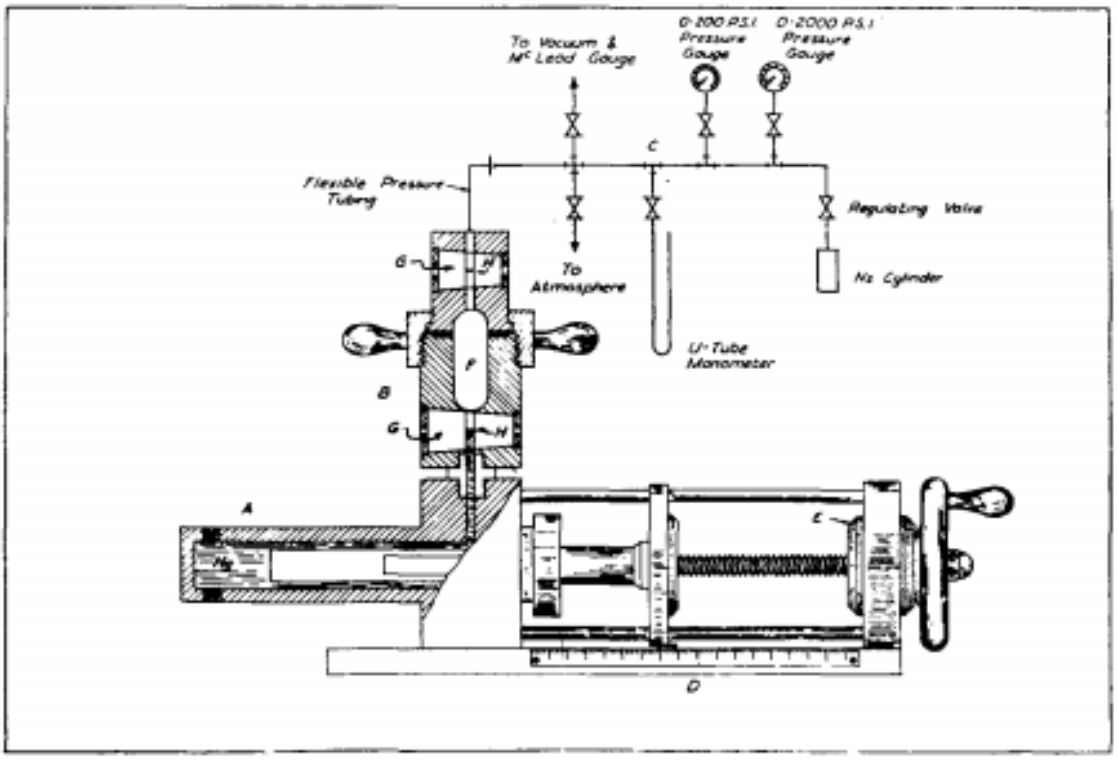

Fig. 8. Apparatus for determining mercury capillary pressures. (Purcell 1949)

Figure 8 represents the apparatus used for determining the mercury capillary pressures in the study conducted by Purcell. Purcell's mercury injection method involves drawing vacuum on the system to remove all the gases prior to mercury injection. Once the vacuum condition is achieved, and the pressure inside the system drops to the desired level, mercury is slowly injected in the system so as to fill up the entire chamber. There are two ways of introducing mercury into the system. In continuous mode, mercury enters the sample at continuously increasing pressure. While in incremental mode, pressure is applied in steps allowing equilibrium at each step of mercury intrusion. Various modified

mercury injection permeability models have been introduced over the years by the contributions of different authors like Thomeer, Winland, Huet, Dastidar, Swanson and Buiting-Clerke, etc. Figure 9 represents the capillary pressure curves used by different authors for determining pore dimensions

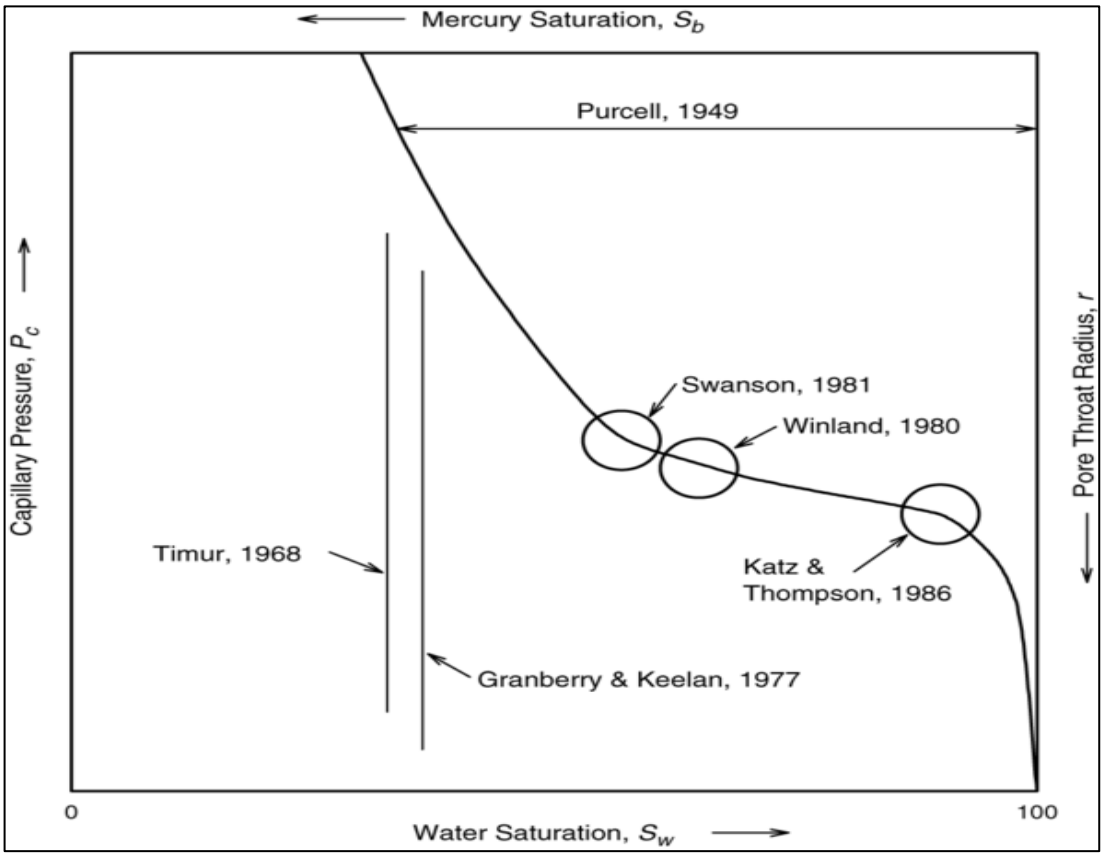

Fig. 9. Capillary pressure curve determining pore characteristics (http://petrowiki.org/Estimating_permeability_based_on_pore_dimension)

Swanson (1981) provided a simple correlation between permeability and mercury capillary pressure. This method picks the maximum ratio of mercury saturation to pressure $(S_b/P_c)^c_{max}$ from the capillary pressure curve on the basis that all connected spaces are filled with mercury and the capillary pressure corresponds to pore sizes

interconnecting the whole system thereby dominating fluid flow. Swanson gave a simple equation in the form of:

$$\mathbf{K = a(S_b/P_c)^c_{max}}$$

Where,

a, c = constants depending on rock type, fluid type,

S_b = Mercury saturation as percent of bulk volume and

P_c = Value related to pore throat radius r

Nooruddin (2016) determined the coefficients of various models using regression techniques. The original and adjusted coefficients were used to obtain permeability which was then validated with the actual data. It was found that the original coefficients generate high error when implemented in the model. The results improved tremendously after the permeability model was used with calibrated coefficients.

2.3.3 Pressure Pulse Decay

Brace et.al (1968) introduced the pulse decay technique for measuring the permeability of granite rocks. Figure 10 shows the schematic of the experimental setup used by Brace:

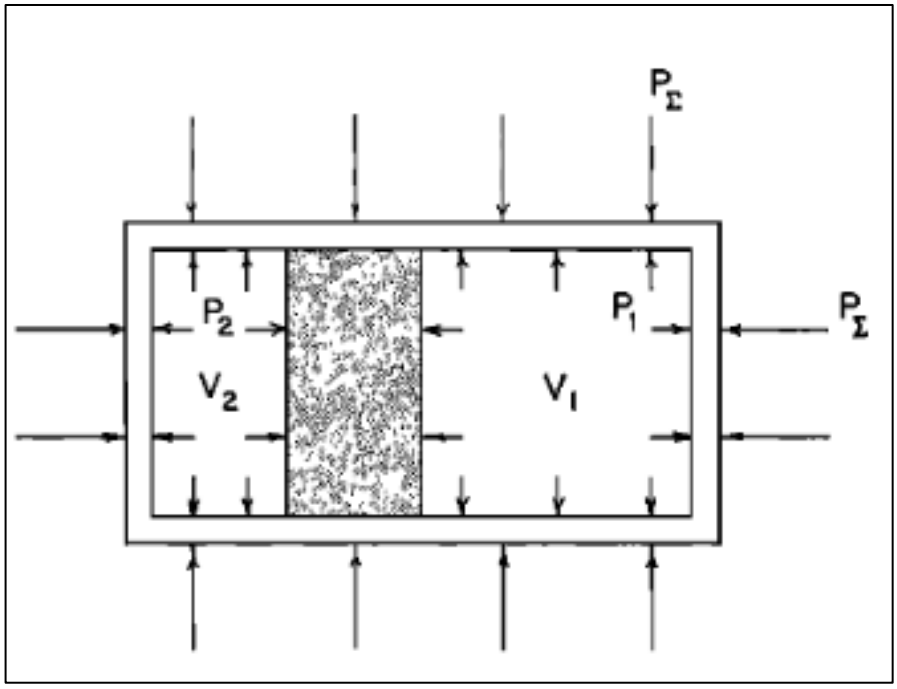

Fig. 10. Schematics of Pulse decay (Brace 1968)

The same method can be applied for measurement of permeability in tight formation rocks with permeability in the range of nano-Darcy. In this method, confining pressure is forced on the rock to attain equilibrium pressure.

Subsequently, a pressure pulse is applied on the upstream end of the rock. The rate of pressure buildup and pressure decay is recorded on the upstream and downstream end of the sample. The recorded data is then analyzed to estimate the permeability of the rock sample. From the recorded data, it is evident that the pressure gradient will decay exponentially to zero.

The following equation can be used to obtain the pressure (P_1) in the reservoir:

$$(\mathbf{P_1 - P_f}) = \mathbf{\Delta P}\left[\left(\frac{\mathbf{V_2}}{\mathbf{V_1}}\right) + \mathbf{V_2}\right]\mathbf{e^{-\alpha t}}$$

Where,

$$\boldsymbol{\alpha} = \left(\frac{\mathbf{kA}}{\mu\boldsymbol{\beta}\mathbf{L}}\right)\left(\frac{\mathbf{1}}{\mathbf{V_1}} + \frac{\mathbf{1}}{\mathbf{V_2}}\right)$$

A = Cross sectional area

L = Length of the sample

V_1, V_2 = Volume of the reservoirs

P_f = final pressure

ΔP = step change in pressure at t = 0

As depicted in Fig. 11, a plot of $P_1 - P_f$ on the logarithmic scale against linear time scale is generated to obtain the slope of the line. . The slope of the line, α, obtained from the plot is used along with the equation above to obtain permeability, k.

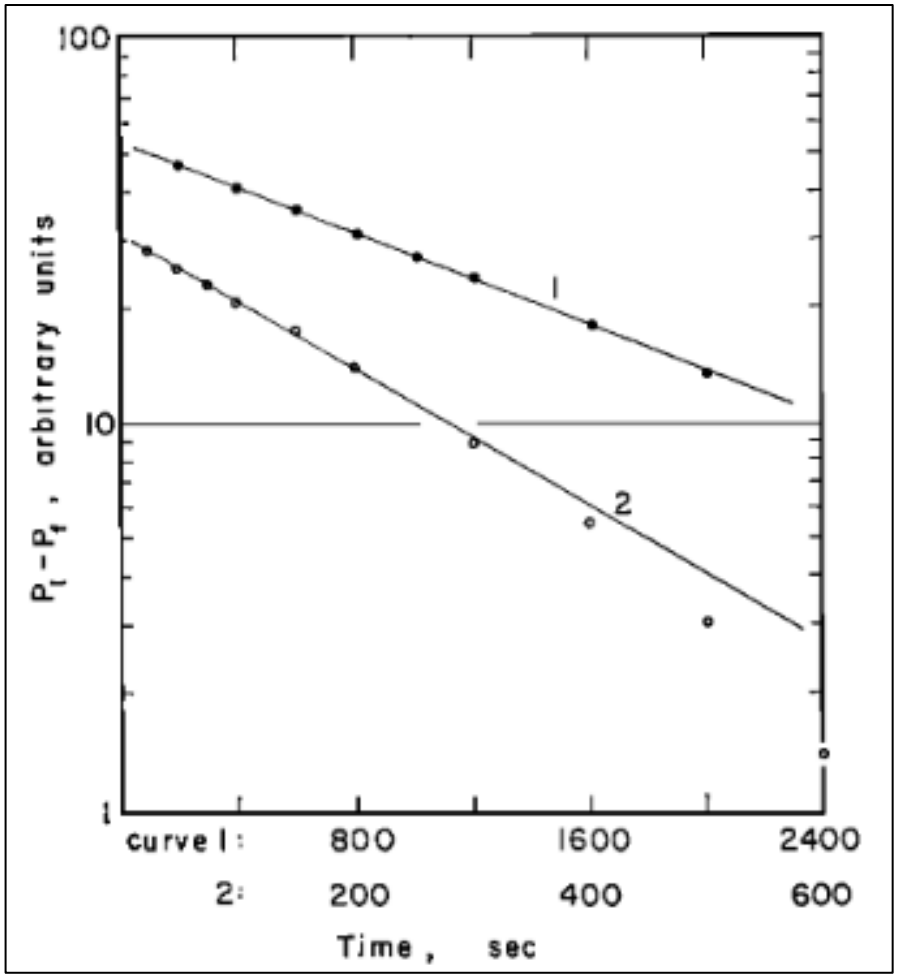

Fig. 11. Sample Decay Curve (Brace 1968)

Zhang (2013) used the same principle as used by Brace et.al. and applied the pressure decay model to get permeability measurements with the added effect of temperature, viscosity and compressibility of nitrogen. Figure 12 shows the pressure decay curve observed on the siltstone sample:

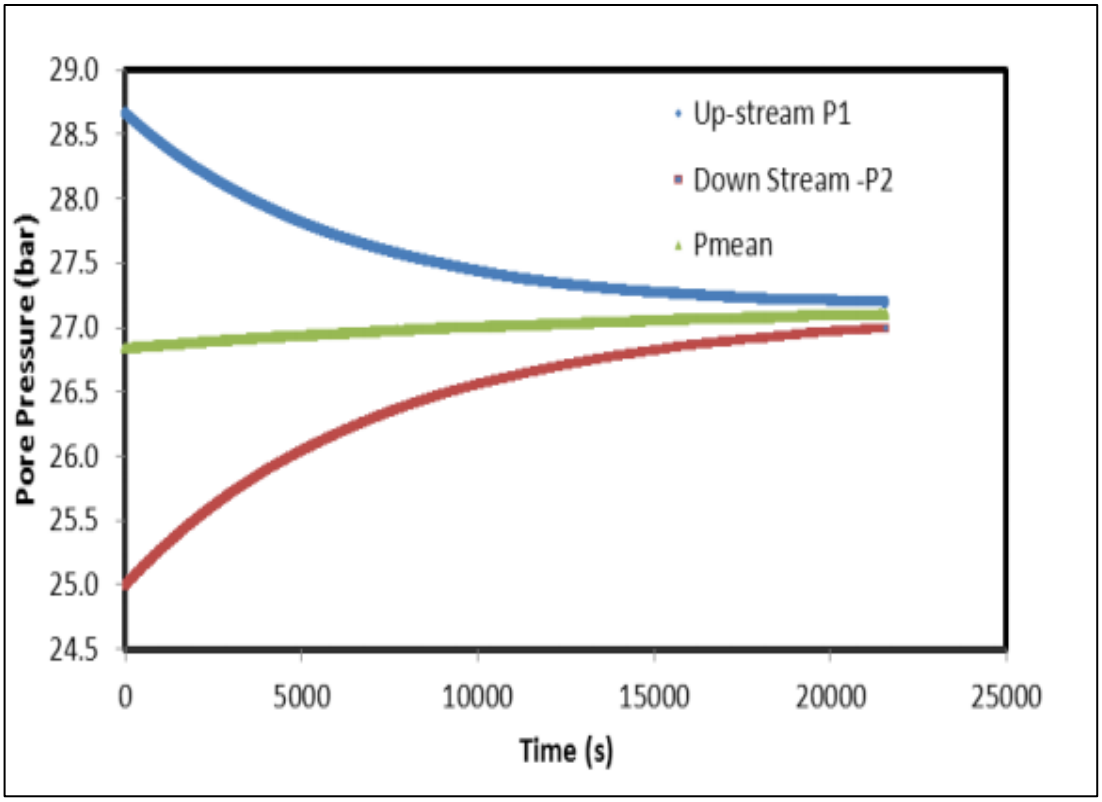

Fig. 12. Pressure upstream, downstream and mean pore pressure (Zhang 2013).

The compressibility β of nitrogen was calculated from the compressibility factor shown below:

$$\mathbf{Z = \frac{PV_m}{RT} = 1 + \frac{B}{V_m} + \frac{C}{2V_m} + \cdots}$$

Where,

P = Pressure, psi

T = Temperature in Farhaneit

R = Gas constant

B, C … = Virial coefficients that are function of temperature

The coefficient B can be obtained by equation of the form:

$$\mathbf{B = a - b\ exp\{c\left(\frac{K}{T}\right)\}}$$

where,

K = Permeability in millidarcy

a = 185.4;

b = 141.8;

c = 88.7.

For all the above explained methods, pressure is the critical factor required to determine any permeability estimates. These methods also need fairly expensive equipment like core holder, pressurized cylinders etc. The current study evaluates the alternative approaches to design an apparatus for conducting experiments in order to attain the same objective at a reduced cost by bypassing the need of costly equipment and incorporating the principle of osmosis and diffusion. The next chapter focuses on the principle behind this investigation.

2.4 Osmosis and Diffusion.

When two different solutions having different concentrations of a phase are separated by a semi-permeable membrane, there will be movement of particles from area of higher concentration to area of lower concentration as shown in Fig. 13. This movement of particles is explained by osmosis and diffusion phenomena.

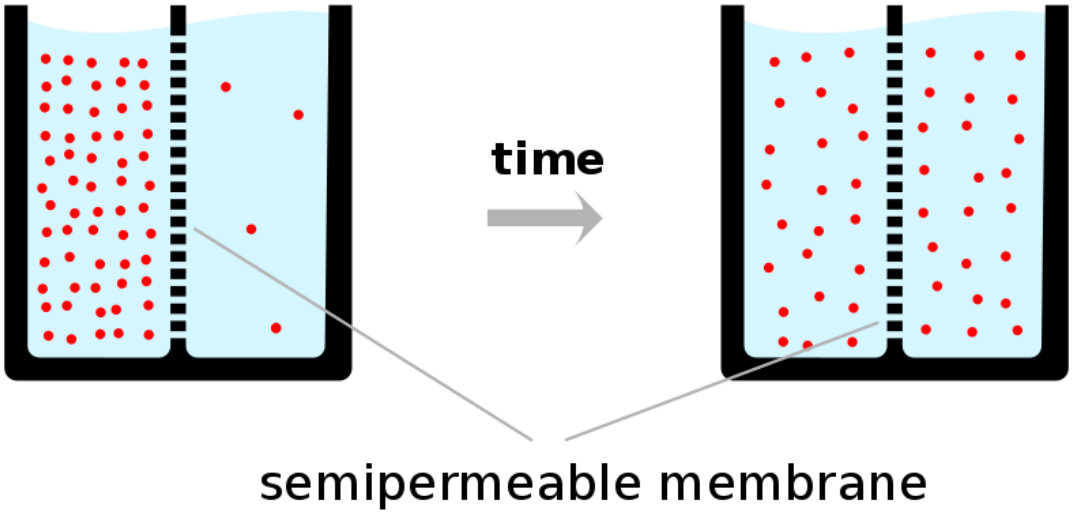

Fig. 13. Osmosis and Diffusion (http://apocketmerlin.tumblr.com/post/15019772012/exchange-across-plasma-membranes-diffusion)

. During drilling, osmotic forces will develop and will cause the movement of water in or out of the shale formation if there exists a water activity imbalance between shale pore fluids and drilling fluid (Mody et.al. 2002). This movement of water and ions in or out of shale is one of the major reasons for shale instability. Even though, osmosis has been a problem to deal with, it can be used to our advantage in order to study the flow properties of the rock sample.

Until recently, the oil industry tackled the movement of water and ions into the shale using oil based muds. Due to its low permeability and the presence of a threshold capillary entry pressure between oil based muds, there exists a restriction on the flow of water into and out of shale, which helps in preventing shale instability. However, due to the higher cost and their negative environmental impact, there is a growing interest to develop water-based muds, which can work as effectively as the oil-based muds. An ideal semipermeable membrane allows the movement of water and restricts the movement of ions (Van Oort., 1994). A number of researchers have concluded that shale does not act as an ideal semi-permeable membrane and that it is more polyporous. Hence, the concept of membrane efficiency was introduced. Membrane efficiency is a measure of how efficiently shale can prevent the movement of ions. Shale, acting as a perfect membrane with 100% efficiency, would restrict the movement of ions completely. On the other hand, if shale allows all the ions to pass through it, its membrane efficiency is 0%.

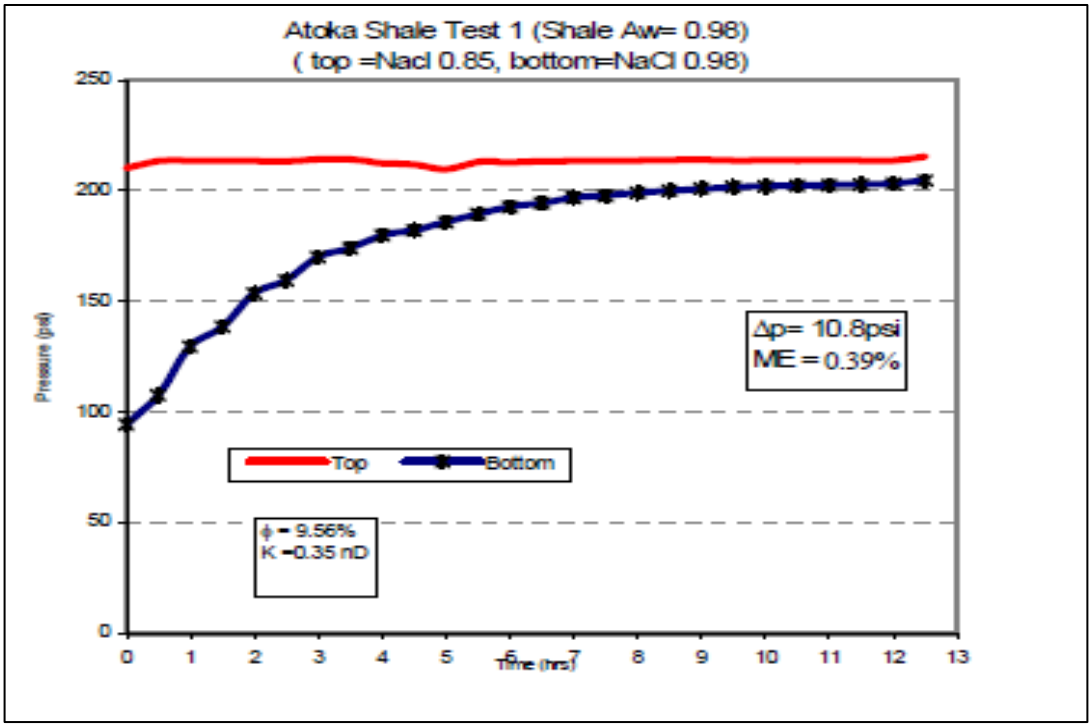

Fig. 14. Pressure Vs Time for Atoka Shale. (Osuji and Chenevert 2008)

Osuji and Chenevert (2008) studied that the membrane efficiency is a function of porosity and permeability of the shale. Pressure transmission test was employed to measure the membrane efficiency of Atoka shale at different porosities as shown in Fig. 14. One of the major conclusions of this study was that the interaction of shale with different water based muds changes the membrane properties of the shale. Two sets of test fluids were studied, one being the brine solution and other the water based mud. For brine solution, it was experimentally concluded that the membrane efficiency is negatively correlated with the shale porosity up to porosity of 7.5%. Beyond this, the change in membrane efficiency is negligible. A good correlation between the shale permeability and membrane efficiency was also obtained.

Majority of the pressure transmission techniques used in laboratory scale experiments are time consuming and require special high pressure apparatus to calculate the membrane efficiency.

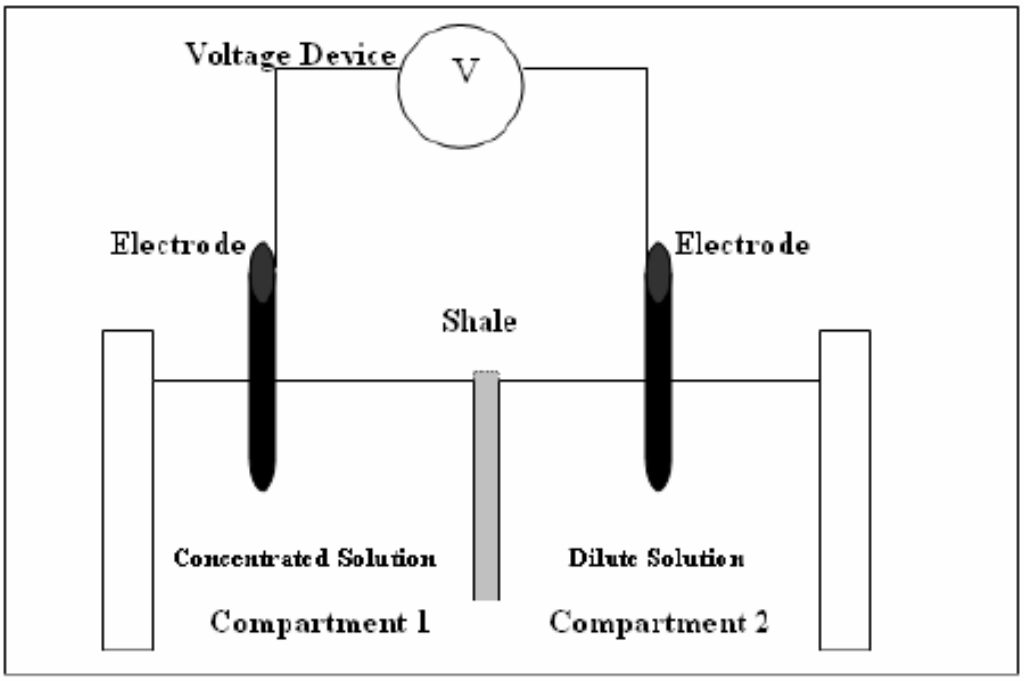

Fig. 15. Schematic of the electrochemical potential test equipment. (Bazali 2005)

Al-Bazali (2005) introduced a new method to obtain the membrane efficiency of the shale cuttings using electrochemical test. Figure 15 is the schematic of the electrochemical test apparatus. It was observed from these tests that the membrane potential is proportional to the ratio of cation exchange capacity and the permeability of shale. It was also concluded that the membrane efficiency of shale is correlated with the ion selectivity. The ion selectivity depends on the type and concentration of cation and anion of the external solution. Figure 16 is a plot of rate of voltage drop measured across the shale membrane.

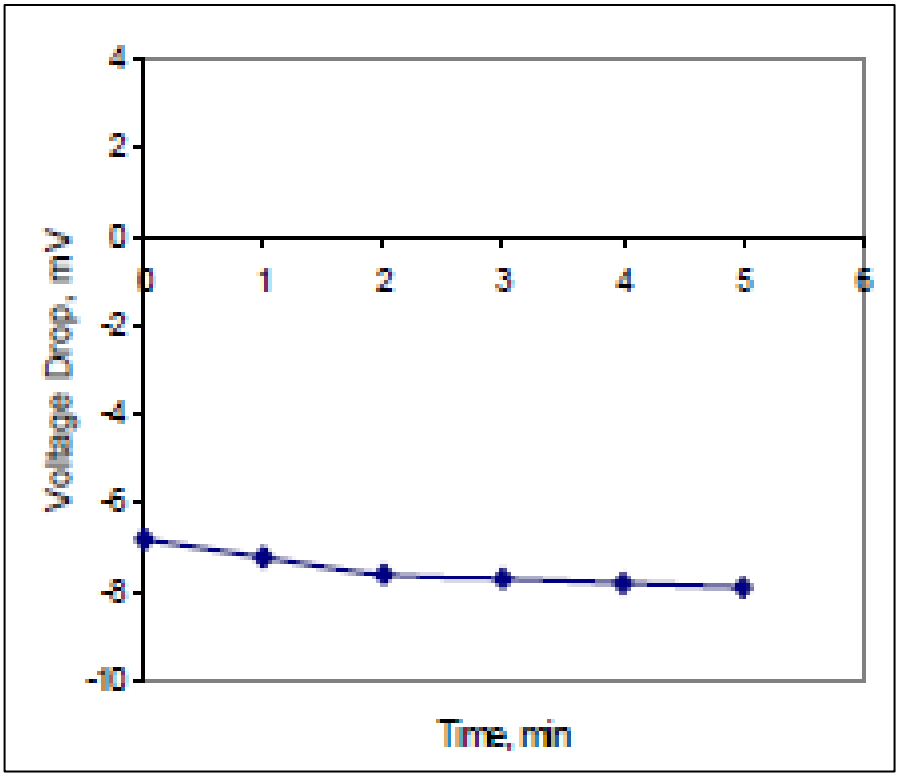

Fig. 16. Voltage drop measurement for Shale during interaction with NaCl solutions. (Bazali 2005)

Lomba and Chenevert (1998) conducted electrochemical experiments to study the membrane behavior of native shales. Figure 17 is the plot of membrane potential developed across shale against the concentration ratio of NaCl solutions.

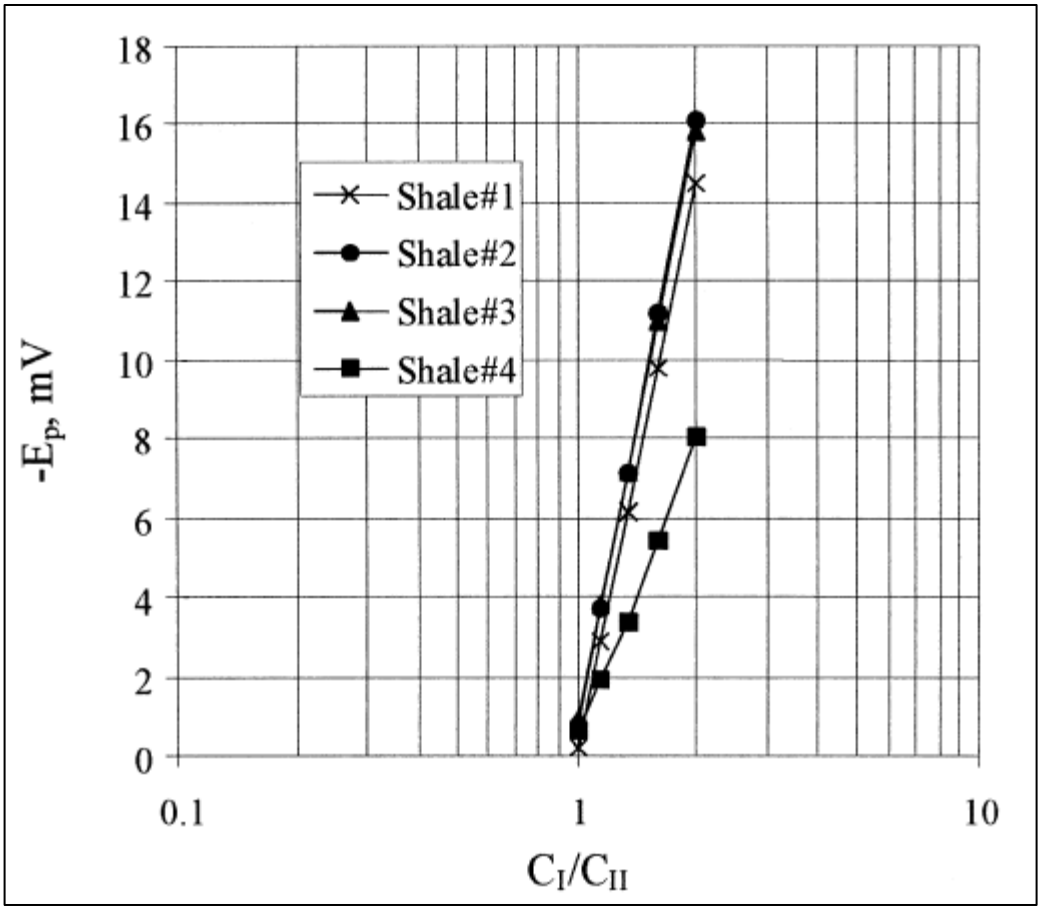

Fig. 17. Membrane potential developed across shale vs concentration ratio of NaCl solutions (Lombart and Chenevert)

It was observed that the composition of the interstitial pore fluid plays an important role in developing electrochemical potential. A model to simulate the transport of water and ions through the shale was also developed. It was concluded that the hydraulic pressure, the concentration and the electrical potential gradients are the critical factors that drive the flow of water and solute across the shale. The modified diffusion potential and the reflection coefficient were calculated from the model to analyze the membrane behavior of shale. The membrane efficiency of the shale was dependent on the concentration of the interstitial fluid, the spacing between the platelets and the type of ions in the membrane. Although this model is an effective way to study the membrane behavior of shale, further

experimental work is required in order to evaluate the membrane efficiency of shale qualitatively. The next chapter discusses the methodology behind the experiments which includes the sample preparation and the test procedure.

3. METHODOLOGY

3.1 Sample material and Sample preparation

Samples from formations like Indiana Limestone, Sister Berea Sandstone, Grey Berea Sandstone and Shale were used in these experiments. Initial tests conducted involved core samples having a length and diameter of 1-in. To reduce the experimental duration, the length was reduced to half in the next set of tests. However, the duration for each experiment was still not reduced significantly and hence, it was finally decided to run experiments with sample length of 0.1-in. or lower, as required. The samples were cut from a 12-inch cylindrical block and dried in the oven for a period of 24 hours. Once dried, the length, diameter and weight of the samples were recorded. Sealants used to prevent the flow of fluid across the circumferential surface area of the sample were epoxy putty and wax. It was observed that wax is much more effective to obtain better seal and hence, most of the tests were carried out with wax as the sealant. Figure 18 is an illustration of the waxing process being carried out on a rock. The waxed samples were then weighed and saturated in separate setup described later in this chapter.

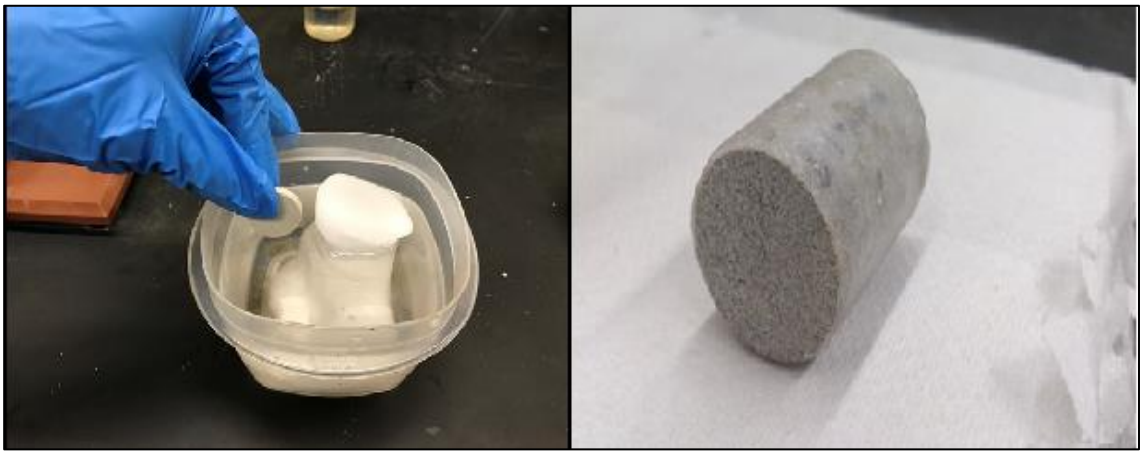

Fig. 18. Waxing in progress (Left) Waxed Sample (Right)

3.2 Test Equipment

Figure 19 shows the schematic of the experimental setup.

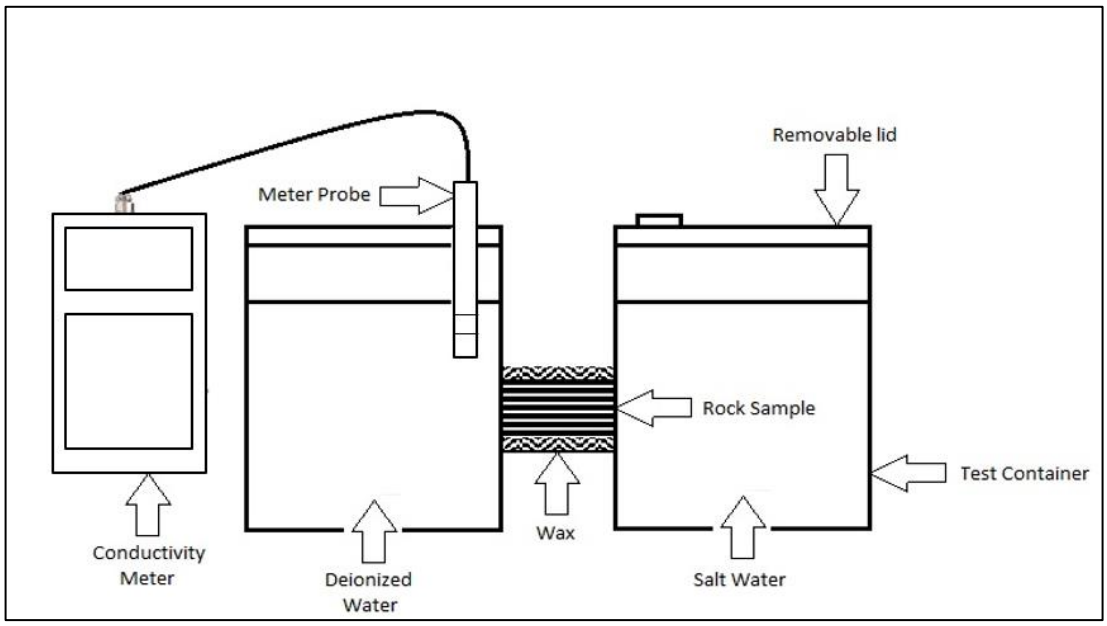

Fig. 19. Schematic of the Experimental Setup

The following section describes the test equipment used and its functions:

Test Container

Figure 20 shows the Kartell 250 ml beakers that were used. These were specifically the desired beakers as they are chemically resistant to most acids, bases and many common solvents. The removable lids were from the mainstay mix and serve containers which had an opening on the top for entry of the meter probe. The beakers were drilled with 1-inch diameter holes to provide path for fluid flow through the rock sample as shown in the figure.

Fig. 20. Kartell 250 ml Beaker

Conductivity Meter

Figure 21 shows the Oakton Con 11 Conductivity meter that was used for conductivity measurements.

Fig. 21. Conductivity Meter

These meters are microprocessor-based instruments and are designed to be handy, capable of allowing one-hand operation. Each has a large customized LCD for clear and easy reading. It also has user-friendly features, all of which are accessible through the splash proof membrane keypad.

Saturation Setup

Figure 22 shows the schematic diagram of the setup which was used to saturate the samples with deionized water.

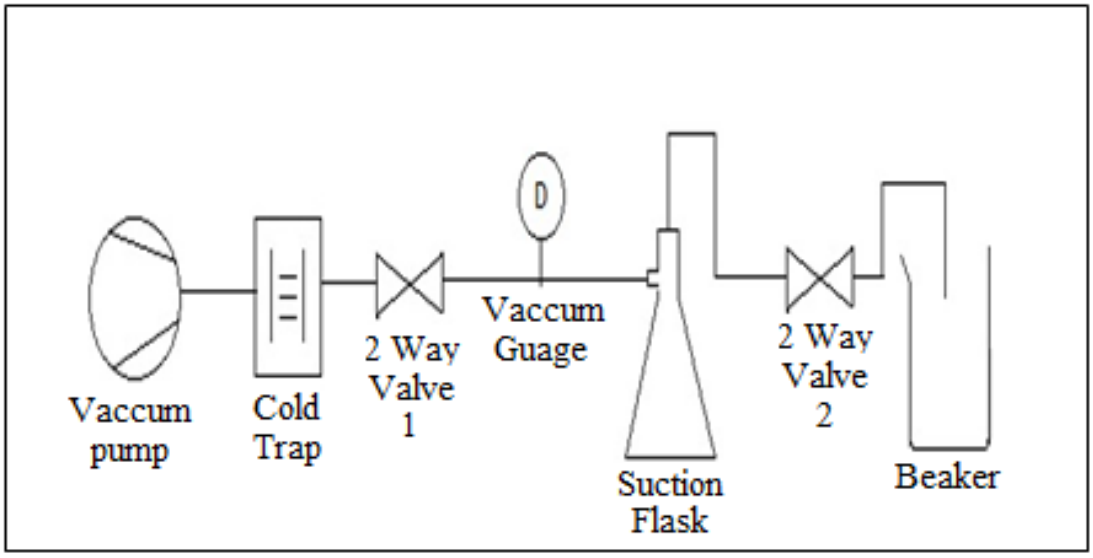

Fig. 22. Schematics of Saturation Setup

The saturation setup consists of a vacuum pump, cold trap, vacuum gauge, suction flask, beaker and two-way valves.

Saturation Procedure

1). Place the Rock Samples to be saturated in the suction flask and close it with the plug as shown in Fig. 23.

2). Keep the Valve 1 in Open position and Valve 2 in the Closed position

3). Switch ON the cold trap. Keep it running for 1 hour. Note the LED on the cold trap turns green indicating it is ready for operation.

4). Switch ON the vacuum pump. Keep it running for 30 minutes. Open Valve 2 slightly to allow deionized water into the tube and close it as soon as it reaches the Valve 2.

5). Keep the vacuum pump running for additional 90 minutes.

6). Put Valve 2 in closed position. Switch OFF the vacuum pump first and then Switch OFF the cold trap. Keep the samples in the suction flask for 24 Hours.

Fig. 23. Saturation in progress

3.3 Test Procedure

Figure 24 show the experimental setup and the test procedure is described in details:

Fig. 24. Experimental Setup

1). Prepare 250 ml 10%wt./wt. KCl solution in a beaker and keep it covered for 12 hours to reach temperature stabilization. Also, store 250 ml of deionized water in a beaker.

2). Heat the wax in the oven for 15 minutes allowing it to melt sufficiently. Take it out and allow it to cool and thicken.

3). Place the saturated rock sample on one inch diameter hole in the beaker and apply wax around its circumference to fix it to the beaker. Allow the wax to harden.

4). Now place the other beaker in a way that it connects the one inch diameter hole to the other end of the rock sample. Again, use wax to seal them together. Note that precautions need to be taken to prevent the wax deposition on the un-waxed area of the rock, Allow the wax to harden. Figure 25 shows the waxed setup.

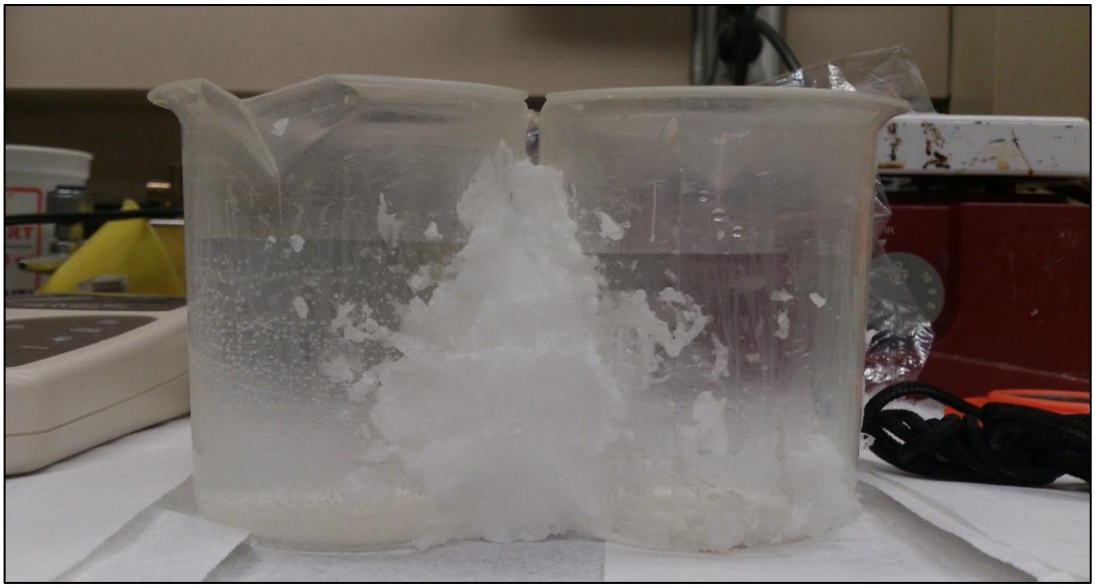

Fig. 25. Waxed Setup

5). Make sure that the two beakers with deionized water, KCL salt solution and a stopwatch are ready before experimental process is initiated.

6). To start the experiment, begin by immersing both the beakers slowly but simultaneously into the waxed setup and start the stopwatch.

7). Record the initial temperature and conductivity with the conductivity meter making sure the marking on the meter probe is completely immersed in the fluid.

8). Note down the readings every 30 minutes and plot the conductivity vs time.

4. RESULTS AND OBSERVATION

This chapter describes the analysis and the results of the experiments that were conducted. The experiments were performed at atmospheric pressure and room temperature. As discussed earlier, the length of the rock samples has a huge effect on the duration required to complete the experiment. The equipment used in the experiments were calibrated before each set of tests. Figure 26 shows the calibration curve observed for the conductivity meter using KCl salt solution

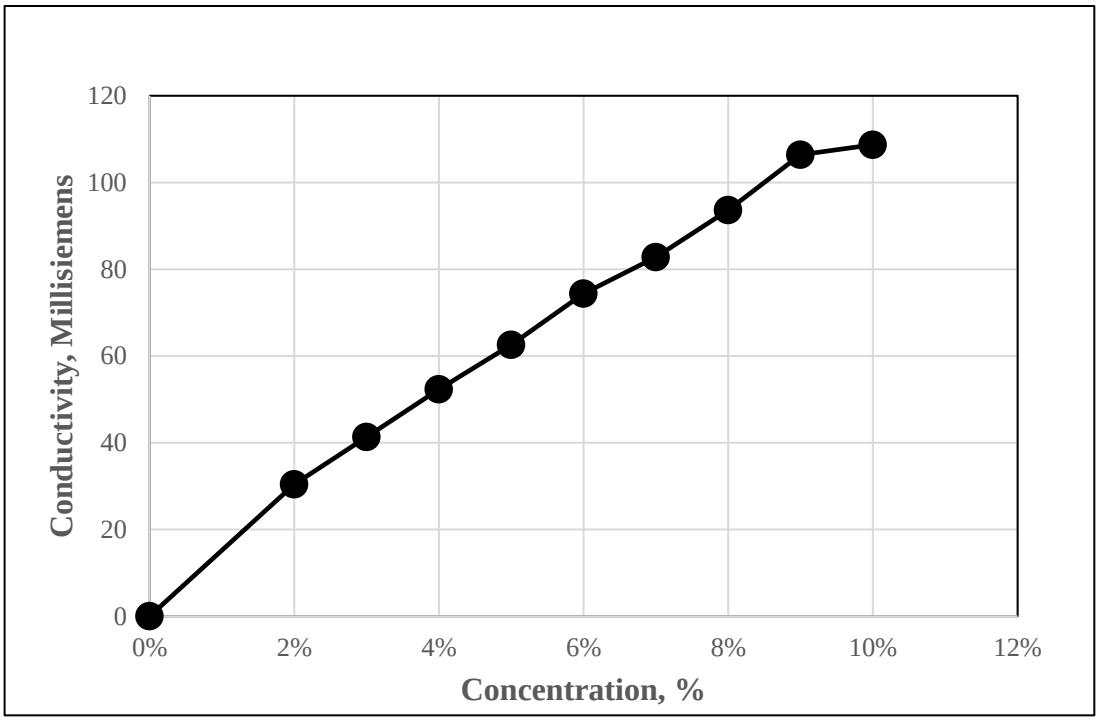

Fig. 26. Conductivity meter calibration using KCl salt Solution

The results of the experiments are discussed in the order they were conducted.

4.1 Indiana Limestone

Indiana Limestone, which is known for its low permeability, was an ideal choice to begin the experimentation. Figure 27 shows the plot of conductivity vs time observed for an Indiana limestone rock sample:

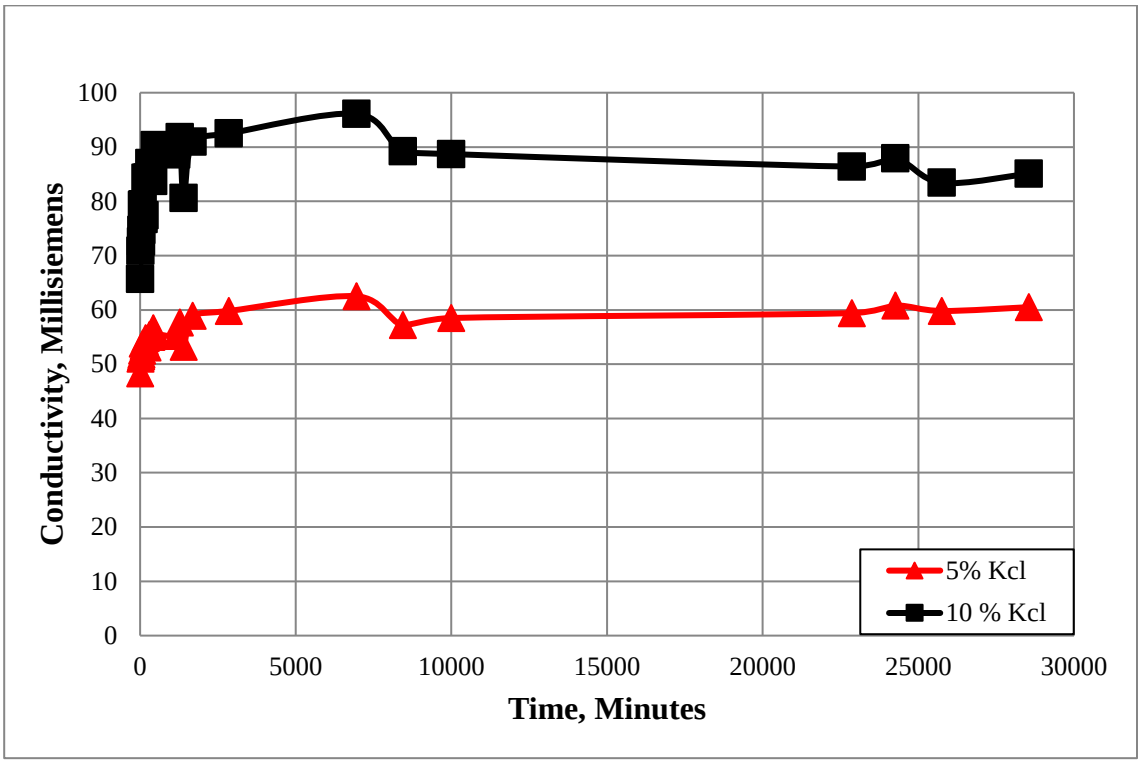

Fig. 27. Conductivity vs time (Indiana limestone - 0.3 inch)

The sample used was a 0.3-in. sample as this experiment was performed in the initial stages and the fluids used were 5% KCl and 10%wt./wt. KCl. It is evident from the plot that there was no sign of diffusion or osmosis between the two fluids even after 30000 minutes (approximately 21 days). The conductivity curve on either side of the rock traces a steady path without any indication of achieving chemical equilibrium. Hence, it was decided, that the permeability of Indiana limestone, which is 2-5 mD, is too low and selecting a higher permeability rock sample for next set of tests was a logical choice.

4.2 Sister Berea Sandstone

Figure 28 to 30 are the plots of conductivity Vs time for sister berea sandstone samples of 0.07, 0.08 and 0.1 inches, respectively. The permeability of the Sister Berea core was recorded as 70 mD. From the respective plots, the occurrence of osmosis and diffusion can be visualized, and hence, it can be concluded that there is movement of particles from 10%wt./wt. KCl solution to the deionized water. On an average, these experiments were allowed to run for 14000-17000 minutes (9 – 12) days. From the overall trend, it is clear that these systems will attain chemical equilibrium.

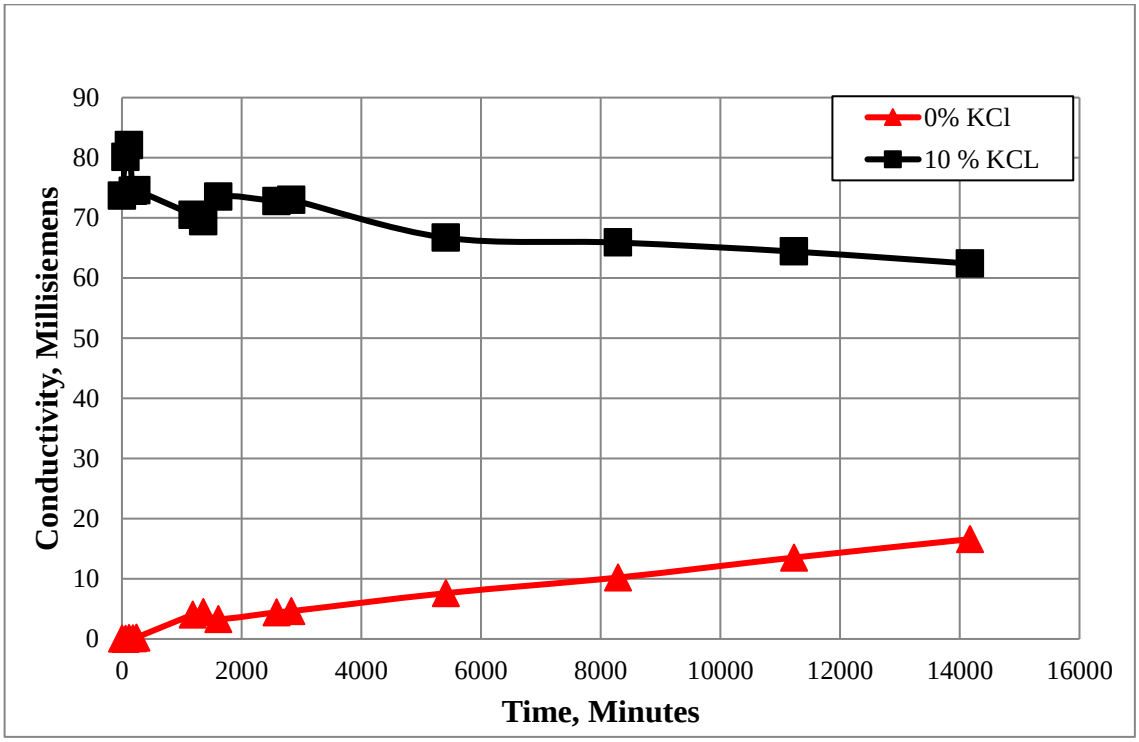

Fig. 28. Conductivity vs time. (Sister Berea - 0.07 Inch)

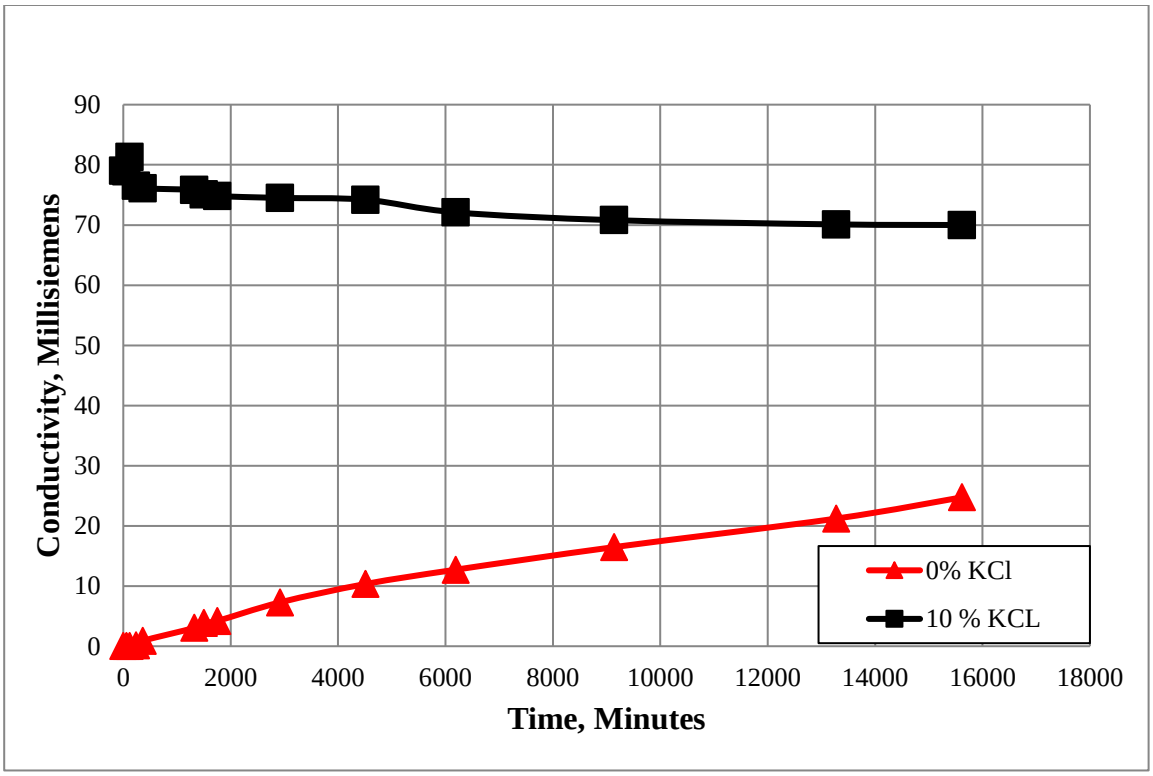

Fig. 29. Conductivity vs time. (Sister Berea 0.08 Inch)

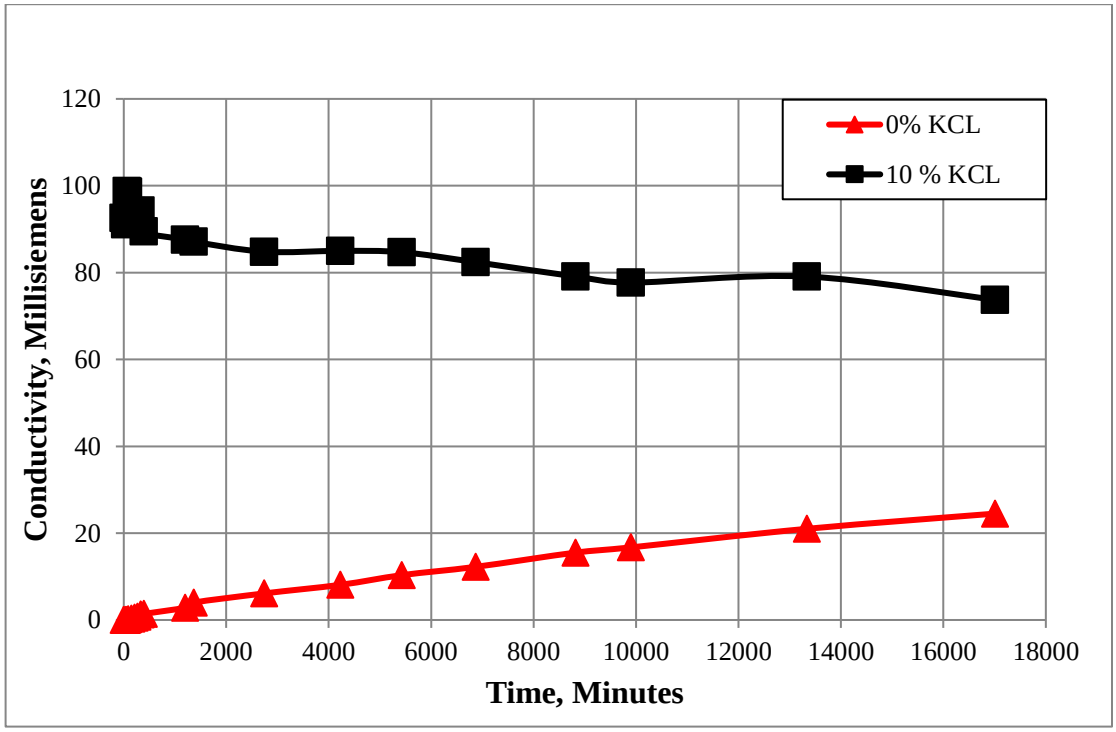

Fig. 30. Conductivity vs time. (Sister Berea - 0.1 Inch)

Figure 31. provides a comparative behavior of the different length of Sister Berea samples. Difference between the conductivities of the fluids is plotted on logarithmic x-axis and the time on y-axis. C_1 represents the conductivity of the deionized water and C_2 represents the conductivity of the 10 % KCl solution. From the plot, it can be observed the slopes of the samples having length 0.07 inch and 0.08 inch follow a similar path and have a different starting point than 0.1-inch sample.

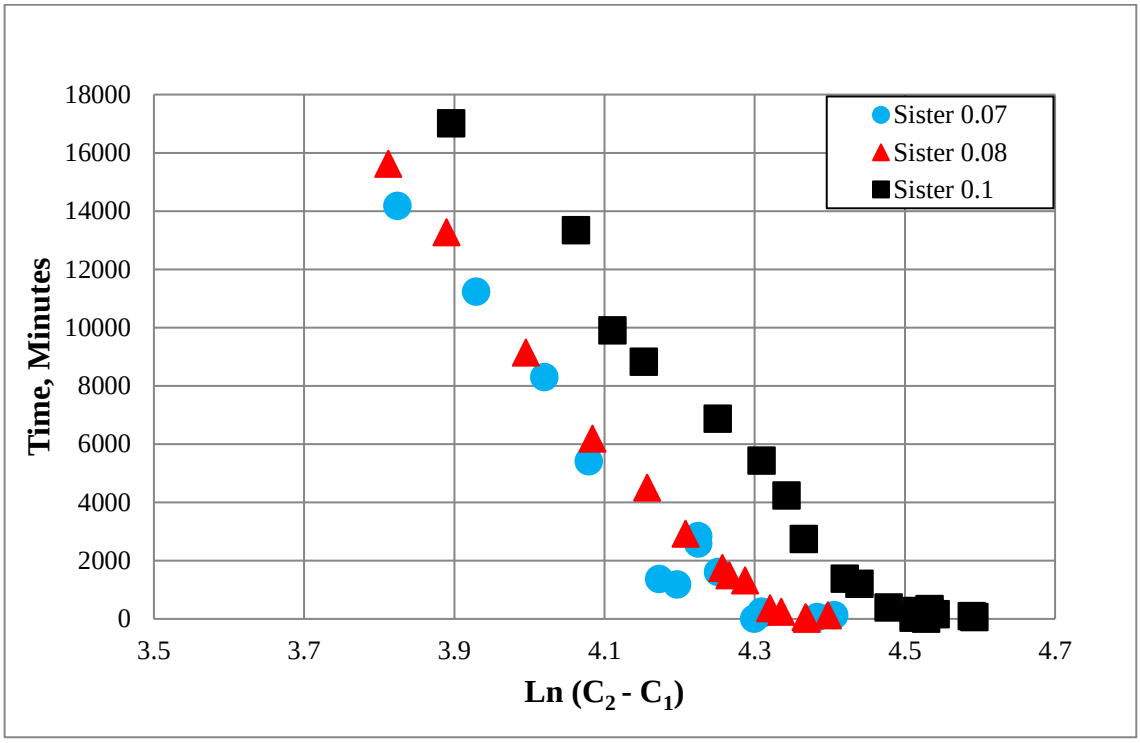

Fig. 31. Sister Berea - Different length comparison

4.3 Grey Berea Sandstone

Figure 32 to 34 shows the plot of Conductivity Vs Time for Grey Berea Sandstone. As in the previous case, the sandstone samples used were of 0.07, 0.08 and 0.1 inches. The permeability of the grey berea core was found to be 130 mD. Similar to sister berea, it can be observed that osmosis and diffusion are taking place, and there is movement of particles from 10%wt./wt. Kcl solution to the Deionized water. On an average, these experiments were allowed to run for 14000-24000 minutes (9 – 17) days. The 0.08-inch sample used was allowed to run for an extended period to find out if there is any change in the trend line. From figure 32, it is clear that the system was still following a steady path towards chemical equilibrium.

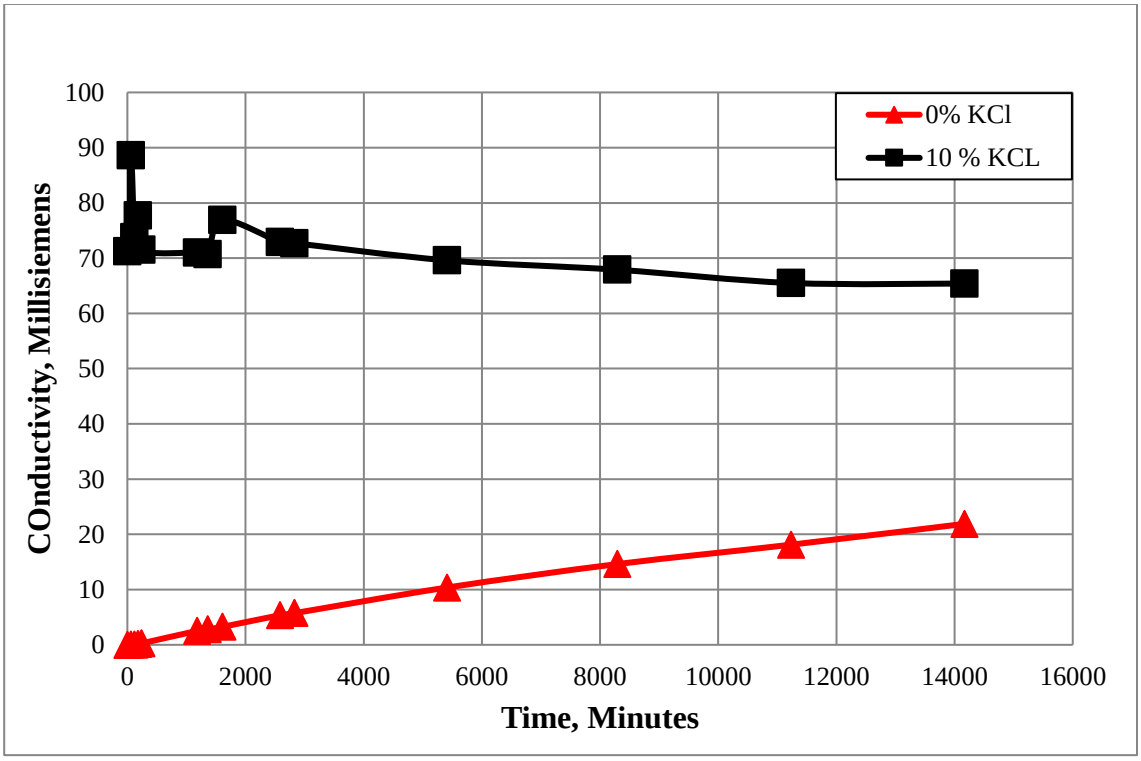

Fig. 32. Conductivity Vs Time. (Grey Berea - 0.07 Inch)

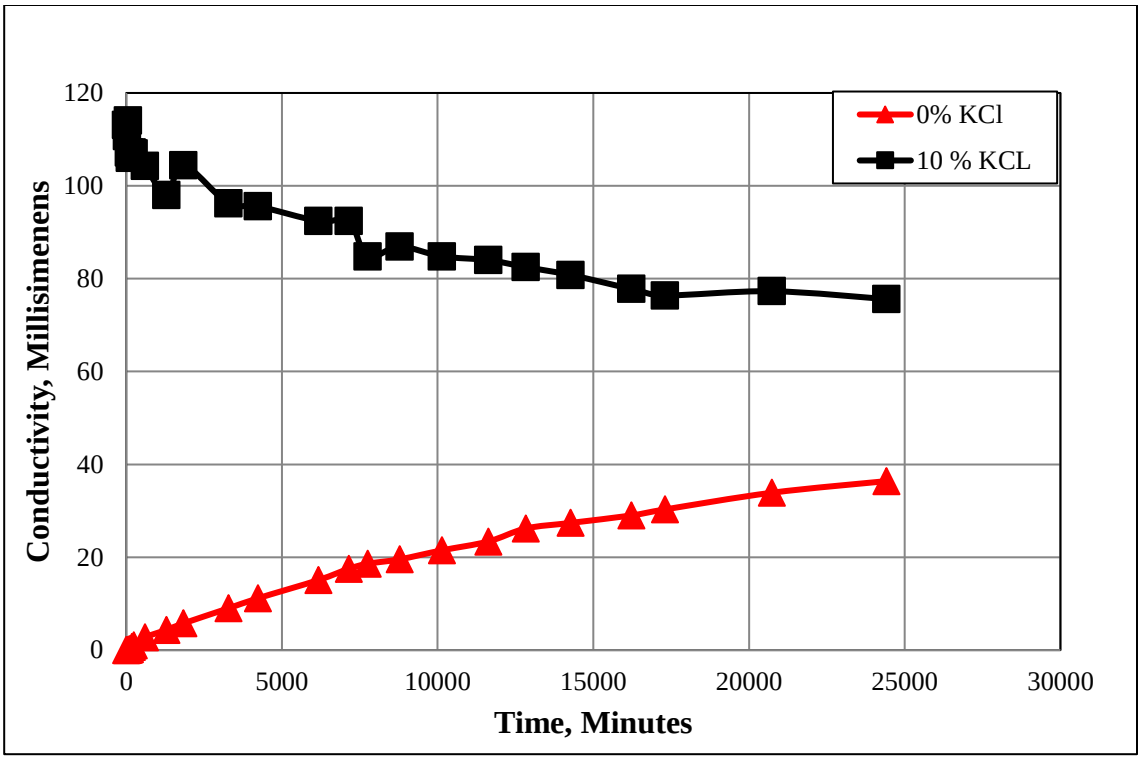

Fig. 33. Conductivity Vs Time. (Grey Berea - 0.08 Inch)

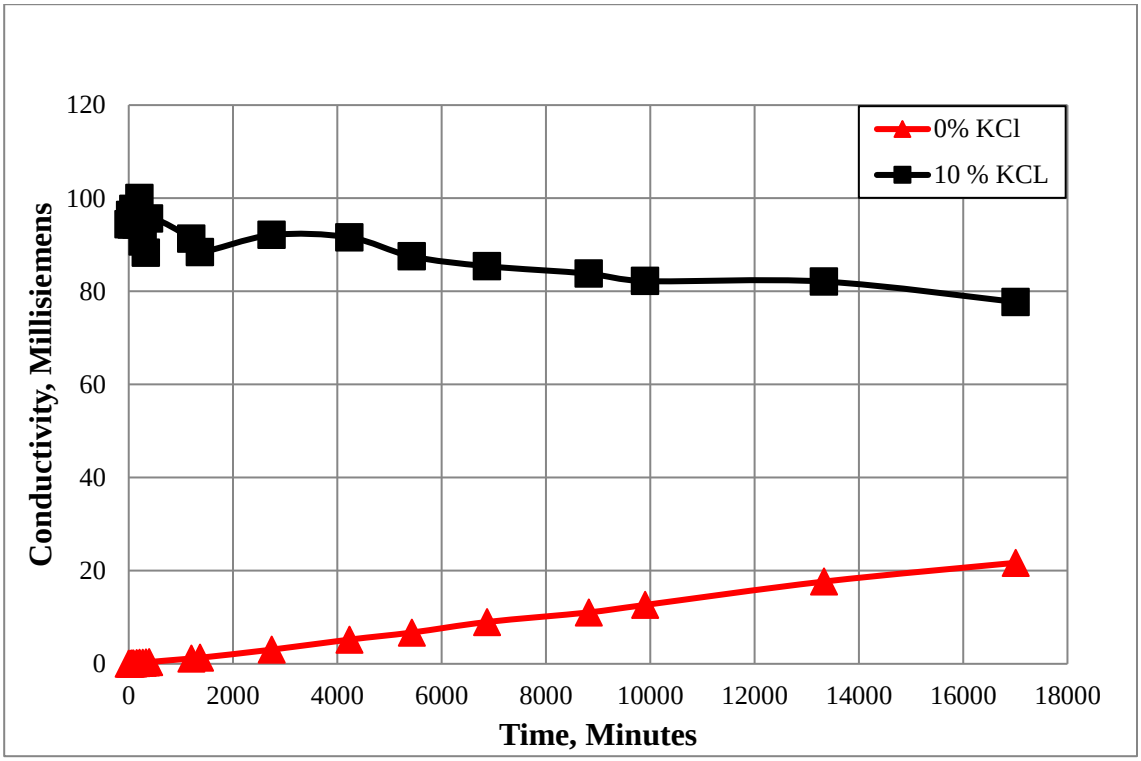

Fig. 34. Conductivity Vs Time. (Grey Berea - 0.1 Inch)

Figure 35 shows the comparative behavior of the different length grey berea samples. On the X-axis, we have the natural logarithm of the difference between the conductivities of the fluids. C_1, is the conductivity of the 10%wt./wt. Kcl solution and C_2 is the conductivity of the deionized water. As compared to sister berea, it can be observed the slopes of the samples having length 0.08 inch and 0.1 inch follow a similar path, but the slope is different while the 0.07 inch and 0.08 inch sample have a similar slope.

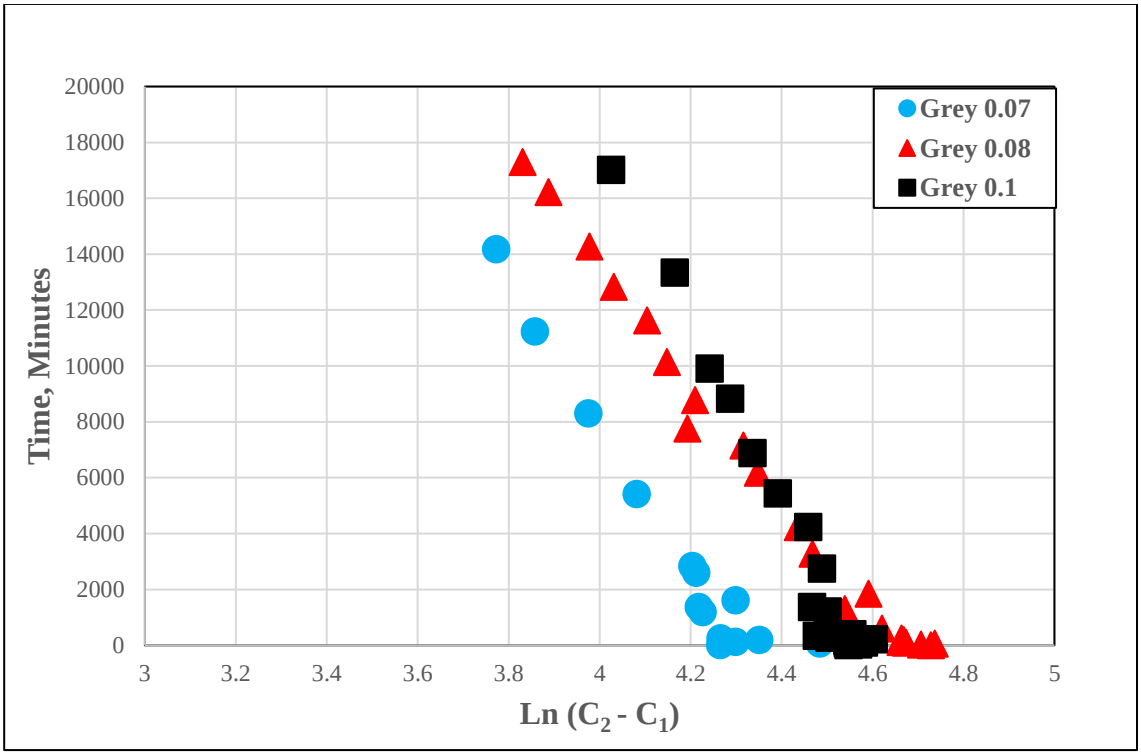

Fig. 35. Grey Berea - Different length comparison

4.4 Sister Berea Vs Grey Berea Sandstone

In this section, we will compare the behavior of both the sister berea and grey berea sandstone of similar lengths. We have already seen the plots of conductivity vs time for different lengths of sister and grey berea sandstone. Figure 36 to 38 shows the plot for same length sister and grey berea sandstones. From figure 36, it can be observed that the plot of Ln ($C_2 - C_1$) vs time for 0.07-inch grey and sister berea follow a similar path with a small difference in slope.

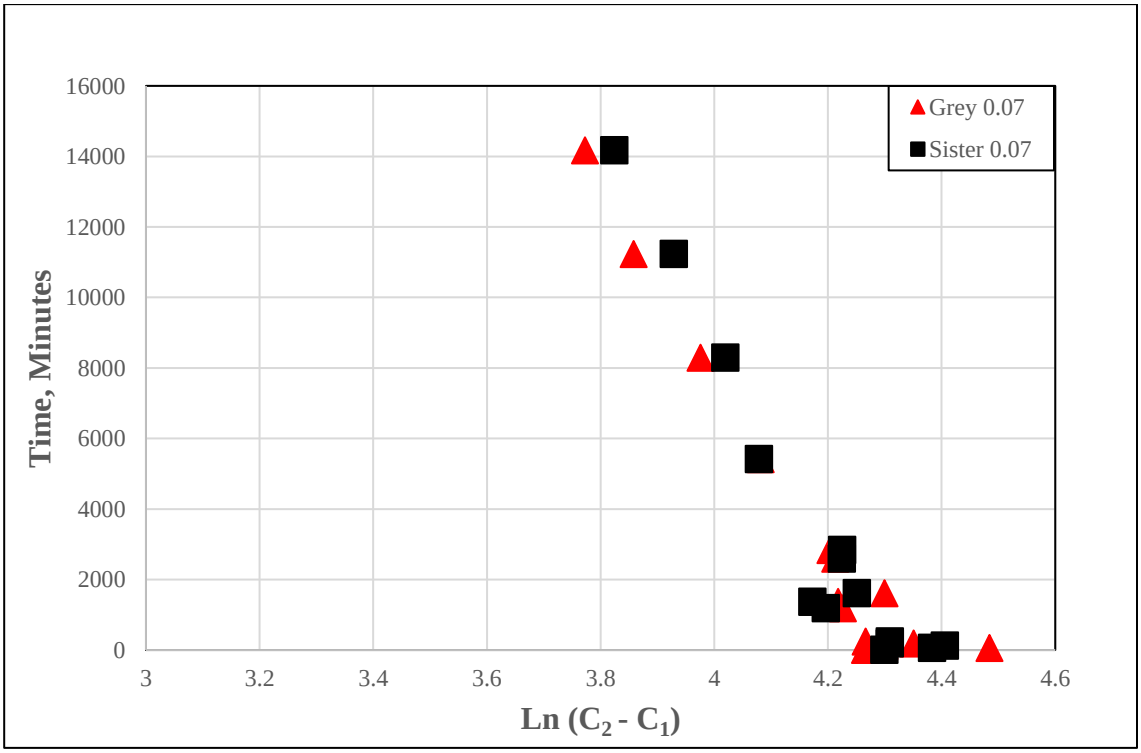

Fig. 36. Grey and Sister Berea - 0.07 Inch

From figure 37, it can be observed from the plot of Ln ($C_2 - C_1$) vs time for 0.08-inch grey and sister, that there is marked difference between the slopes of the two samples. Also, it can be seen that both the samples have different starting points.

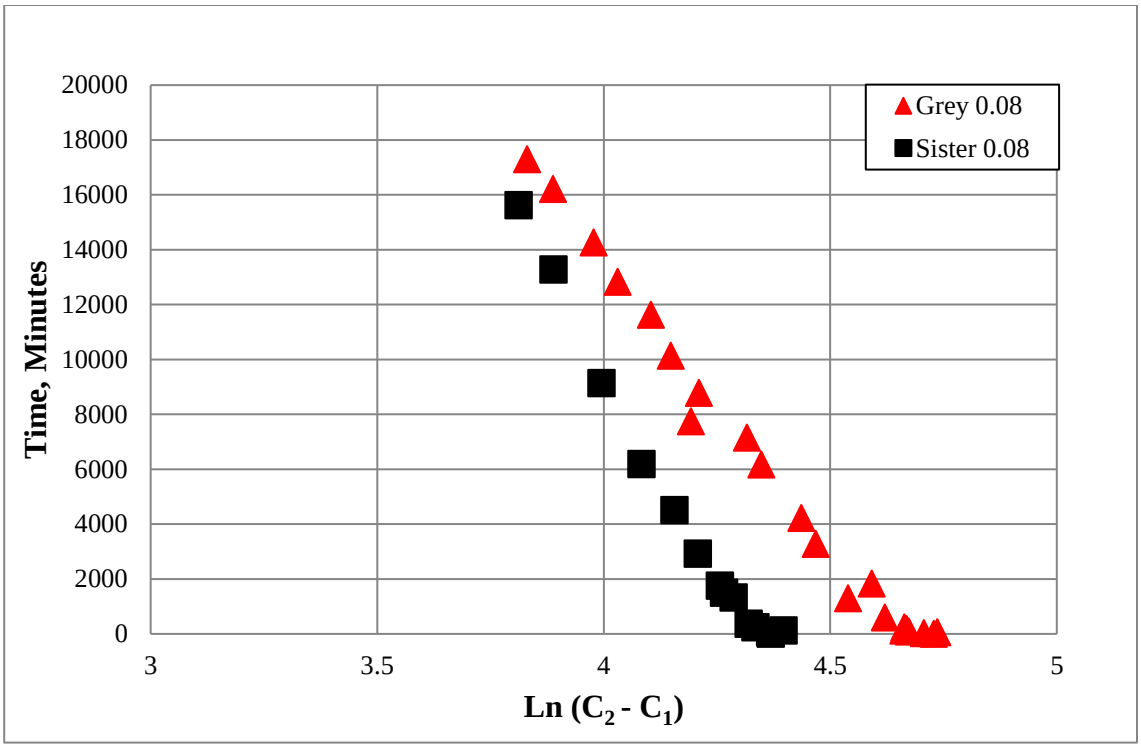

Fig. 37. Grey and Sister Berea - 0.08 Inch

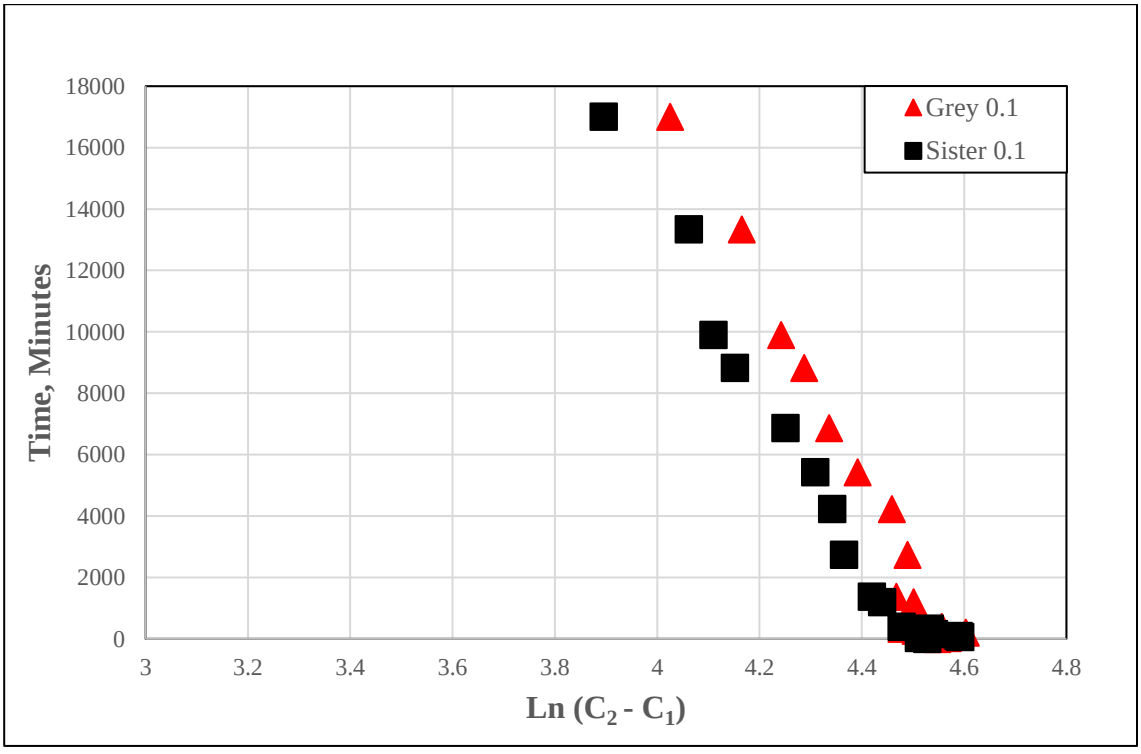

Fig. 38. Grey and Sister Berea - 0.1 inch

From figure 38, it can be seen that the plot trend line is similar to what we observed in 0.07-inch sample. Both the samples have same starting point, the initial trend line moves differently but during later stages the slopes become similar.

4.5 Shale

Figure 39 shows the plot of Conductivity Vs Time for Shale sample. The length of the samples used was 0.08 inches.

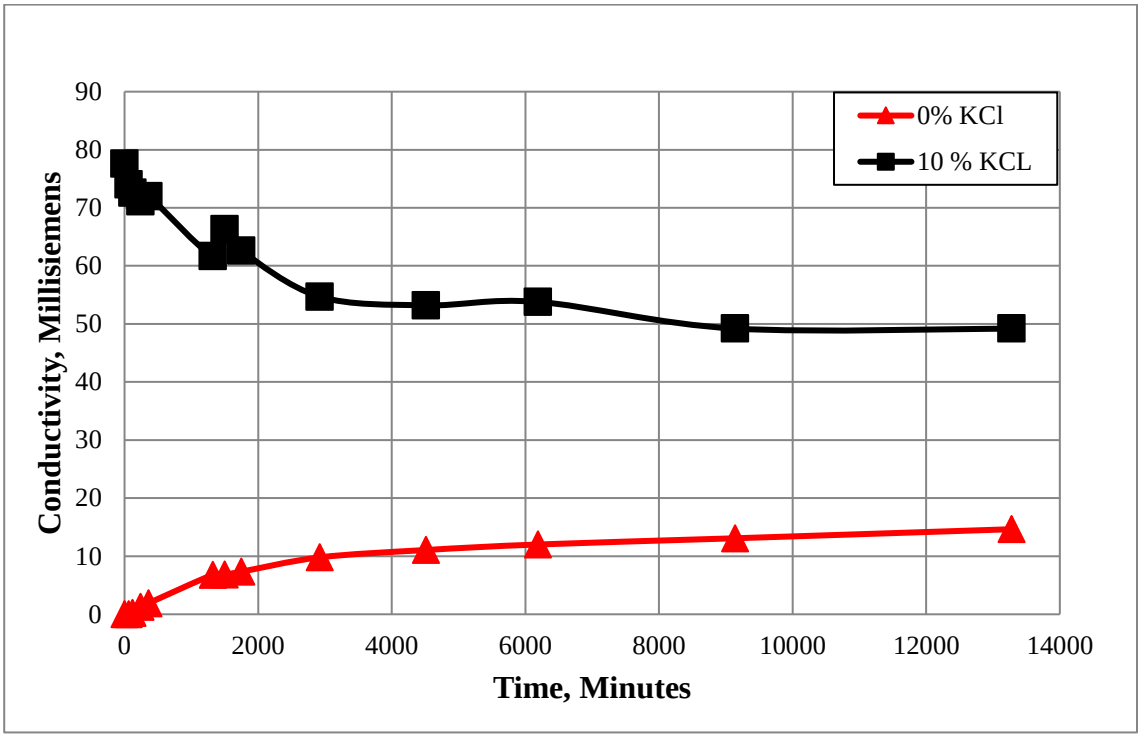

Fig. 39. Conductivity Vs Time. (Shale - 0.08 inch)

The permeability of the shale was found to be 150 nD. Even though shale has lower permeability, it can be observed that osmosis and diffusion are taking place, and there is movement of particles from 10%wt./wt. Kcl solution to the Deionized water. The experiment was allowed to run for approximately 14000 minutes (9 days). It can be seen that, during the initial stages of the experiment, there is a faster convergence between the two fluids. At close to 4000 minutes, the convergence has reached saturation and has

slowed down. The slowdown in the convergence can be seen from 4000 to 13500 minutes. Similar to sister and grey berea, from the overall trend it is clear that these systems will reach chemical equilibrium.

Sister Berea Vs Grey Berea Vs Shale

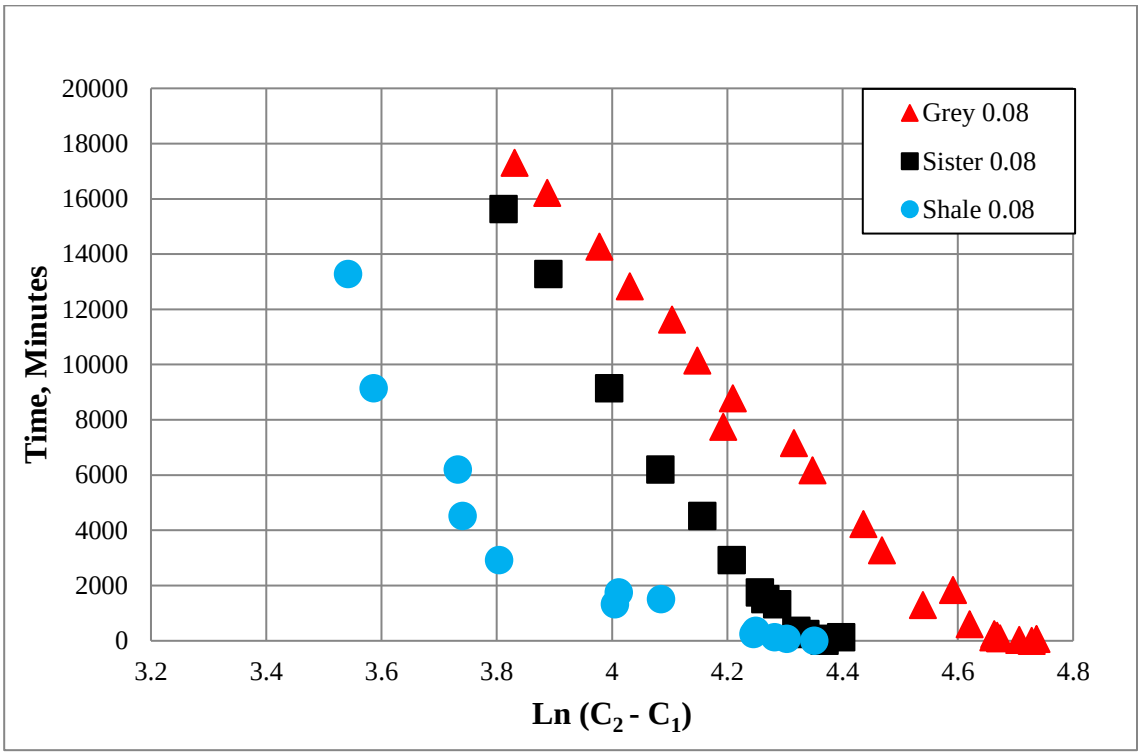

Fig. 40. Comparison between sister berea, grey berea and shale (0.08 inch)

Figure 40 shows the plot of Ln ($C_2 - C_1$) vs time for 0.08-inch grey berea, sister berea and shale samples. From the plot, it can be observed that shale and sister berea have a similar starting point. Figure 41 shows the combine plot of Ln ($C_2 - C_1$) vs time for all the rock samples.

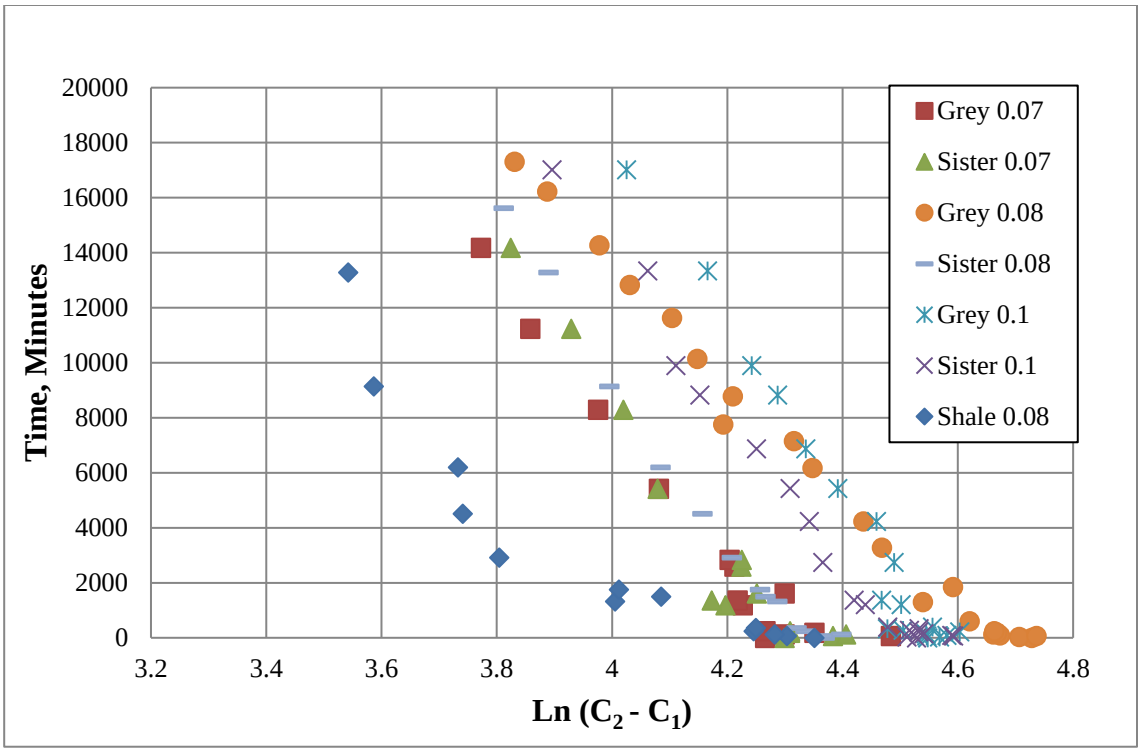

Fig. 41. Comparison between Sister Berea, Grey Berea and Shale (Different lengths)

5. CONCLUSION

The work presented in this study aims to provide an alternative to the more traditional methods for estimating rock permeability in low permeability formations. The following conclusions are drawn:

- The permeability of Indiana limestone is too low (2 – 5 mD) to reach chemical equilibrium.
- Sister Berea and Grey Berea sandstone clearly exhibit the process of diffusion and osmosis. In both cases, movement of particles from higher concentration to lower concentration is observed. Thus, both the systems follow a smooth path towards chemical equilibrium.
- In case of shale, there is an initial phase where convergence occurs at a rapid rate. The movement of particles decelerates at later stages as observed towards the end of the experiment.
- It is also concluded that the length of the rock samples has a huge effect on the time taken by the fluids to reach chemical equilibrium. The shorter the length of the rock sample, the faster it reaches equilibrium.

References

Profice, S., Lasseux, D., Jannot, Y., Jebara, N., & Hamon, G. (2012, December 1). Permeability, Porosity and Klinkenberg Coefficient Determination on Crushed Porous Media. Society of Petrophysicists and Well-Log Analysts.

Kamath, J. (1992, December 1). Evaluation of Accuracy of Estimating Air Permeability from Mercury-Injection Data. Society of Petroleum Engineers. doi:10.2118/18181-PA

Brace, W. F., J. B. Walsh, and W. T. Frangos (1968), Permeability of granite under high pressure, J. Geophys. Res., 73(6), 2225–2236, doi:10.1029/JB073i006p02225

Churcher, P. L., French, P. R., Shaw, J. C., & Schramm, L. L. (1991, January 1). Rock Properties of Berea Sandstone, Baker Dolomite, and Indiana Limestone. Society of Petroleum Engineers. doi:10.2118/21044-MS

Speight, James G. Shale gas production processes. Gulf Professional Publishing, 2013.

http://academic.brooklyn.cuny.edu/geology/powell/613webpage/NYCbuilding/IndianaLimestone/IndianaLimestone.htm

Yaalon, D. H. "Mineral composition of the average shale." (1961).

Zhan, Xin, et al. "Pore-scale modeling of electrical and fluid transport in Berea sandstone." Geophysics 75.5 (2010): F135-F142.

https://malouffbioblog.wordpress.com/2011/11/29/diffusion-and-osmosis-coming-to-a-lab-near-you/

Best, M. E., and T. J. Katsube. "Shale permeability and its significance in hydrocarbon exploration." The Leading Edge 14.3 (1995): 165-170.

Appendix A. Mineralogical and chemical data Geological Society, London, Engineering Geology Special Publications, 21:449-459, doi: 10.1144/GSL.ENG.2006.021.01.16

http://energy.gov/sites/prod/files/2013/04/f0/how_is_shale_gas_produced.pdf

Cao, Cheng, et al. "A new approach for measuring the permeability of shale featuring adsorption and ultra-low permeability." Journal of Natural Gas Science and Engineering 30 (2016): 548-556.

Pathi, Venkat Suryanarayana Murthy. Factors affecting the permeability of gas shales. Diss. University of British Columbia, 2008.

Dewhurst, D.N., Aplin, A.C., Sarda, J.-P. and Yang, Y. 1998. Compaction-driven evolution of porosity and permeability in natural mudstones: An experimental study. Journal of Geophysical Research, v. 103, p. 651—661.

Kwon, 0., Kronenberg, A.K., Gangi, A.F., Johnson, B., and Herbert, B.E. 2004. Permeability of Illite-bearing shale: 1. Anisotropy and effects of clay content and loading, J.Geophys. Res., B 10205, doi: 10.1029/2004JB003052.

Rushing, J. A., Newsham, K. E., Lasswell, P. M., Cox, J. C., & Blasingame, T. A. (2004, January 1). Klinkenerg-Corrected Permeability Measurements in Tight Gas Sands: Steady State versus Unsteady-State Techniques. Society of Petroleum Engineers. doi:10.2118/89867-MS

Sondergeld, C. H., Newsham, K. E., Comisky, J. T., Rice, M. C., & Rai, C. S. (2010, January 1). Petrophysical Considerations in Evaluating and Producing Shale Gas Resources. Society of Petroleum Engineers. doi:10.2118/131768-MS

Zhang, Xiangmin, et al. "Tight rock permeability measurement by pressure pulse decay and modeling." Scaweb. Org (2013): 1-12.

Hasan A. Nooruddin, M. Enamul Hossain, Hasan Al-Yousef, Taha Okasha, Comparison of permeability models using mercury injection capillary pressure data on carbonate rock samples, Journal of Petroleum Science and Engineering, Volume 121, September 2014, Pages 9-22, ISSN 0920-4105, http://dx.doi.org/10.1016/j.petrol.2014.06.032. (http://www.sciencedirect.com/science/article/pii/S0920410514001880)

Purcell, W.R.: "Capillary Pressures-Their Measurement Using Mercury and the Calculation of Permeability", Trans. AIME, (1949), 186, 39.

Swanson, B. F. (1981, December 1). A Simple Correlation between Permeability's and Mercury Capillary Pressures. Society of Petroleum Engineers. doi:10.2118/8234-PA

Nooruddin, Hasan A., et al. "IMPROVEMENT OF PERMEABILITY MODELS USING LARGE MERCURY INJECTION CAPILLARY PRESSURE DATASET FOR MIDDLE EAST CARBONATE RESERVOIRS." Journal of Porous Media 19.5 (2016).

http://apocketmerlin.tumblr.com/post/15019772012/exchange-across-plasma-membranes-diffusion

Mody, F. K., Tare, U. A., Tan, C. P., Drummond, C. J., & Wu, B. (2002, January 1). Development of Novel Membrane Efficient Water-Based Drilling Fluids through Fundamental Understanding of Osmotic Membrane Generation in Shale's. Society of Petroleum Engineers. Doi: 10.2118/77447-MS

Van Oort, E. (1997, January 1). Physico-Chemical Stabilization of Shales. Society of Petroleum Engineers. Doi: 10.2118/37263-MS

Osuji, C. E., Chenevert, M. E., & Sharma, M. M. (2008, January 1). Effect of Porosity and Permeability on the Membrane Efficiency of Shales. Society of Petroleum Engineers. Doi: 10.2118/116306-MS

Talal Mohammad AL-Bazali, (2005). Experimental Study of the Membrane Behavior of Shale during Interaction with Water-based and Oil-based Muds

Al-Bazali, T. M., Zhang, J., Chenevert, M. E., & Sharma, M. M. (2005, January 1). A Rapid, Rigsite Deployable, Electrochemical Test for Evaluating the Membrane Potential of Shales. Society of Petroleum Engineers. Doi:10.2118/96098-MS

Oleas, A. M., Osuji, C. E., Chenevert, M. E., & Sharma, M. M. (2010, March 1). Entrance Pressure of Oil-Based Mud into Shale: Effect of Shale, Water Activity, and Mud Properties. Society of Petroleum Engineers. Doi: 10.2118/116364-PA

Mehana, Mohamed, and Mashhad Fahes. "The Impact of the Geochemical Coupling on the Fate of Fracturing Fluid, Reservoir Characteristics and Early Well Performance in Shale Reservoirs." SPE Kingdom of Saudi Arabia Annual Technical Symposium and Exhibition. Society of Petroleum Engineers, 2016.

Mehana, Mohamed. On the fate of the fracturing fluid and its impact on load recovery and well performance. Diss. University of Oklahoma, 2016.